AD-A068 422 MALLORY (P R) AND CO INC BURLINGTON MASS LAB FOR PH--ETC F/G 10/3
LITHIUM-THIONYL CHLORIDE BATTERY.(U)
APR 79 A N DEY, W BOWDEN, J MILLER, P WITALIS DAAB07-78-C-0563

UNCLASSIFIED DELET-TR-78-0563-1 NL

1 OF 1
ADA
068422

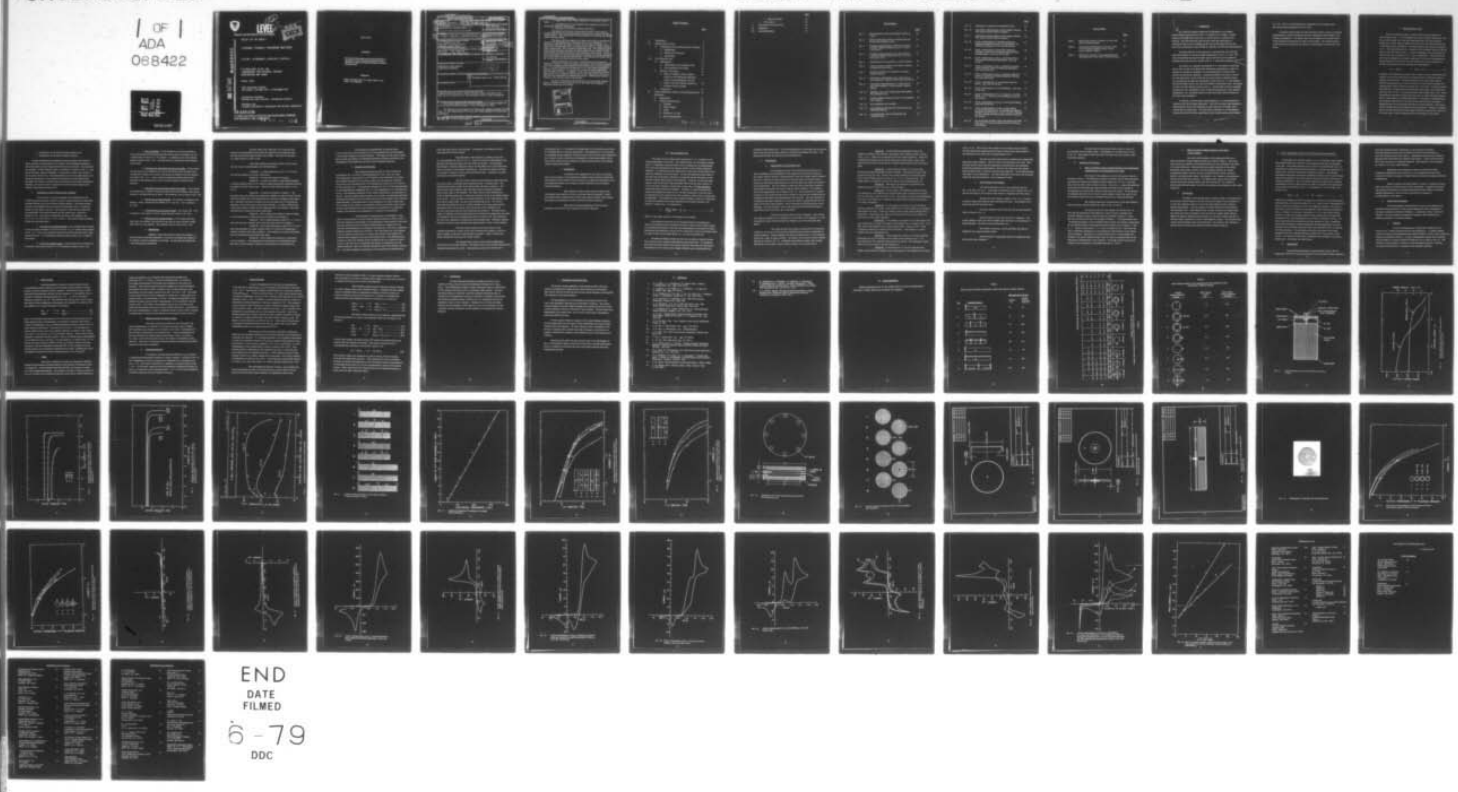

END
DATE
FILMED
6-79
DDC

LEVEL II

Research and Development Technical Report

DELET-TR-78-0563-1

LITHIUM - THIONYL CHLORIDE BATTERY

A.N. DEY , W. BOWDEN , J. MILLER, P. WITALIS

P.R. MALLORY & CO., INC.
LABORATORY FOR PHYSICAL SCIENCE
BURLINGTON , MA 01803

APRIL 1979

FIRST QUARTERLY REPORT
FOR PERIOD 1 OCTOBER 1978 - 31 DECEMBER 1978

DISTRIBUTION STATEMENT :
APPROVED FOR PUBLIC RELEASE ; DISTRIBUTION UNLIMITED

PREPARED FOR :
US ARMY ELECTRONICS TECHNOLOGY AND DEVICES LABORATORY

ERADCOM

US ARMY ELECTRONICS RESEARCH AND DEVELOPMENT COMMAND
FORT MONMOUTH, NEW JERSEY 07703

NOTICES

Disclaimers

The citation of trade names and names of manufacturers in this report is not to be construed as official Government *indorsement or approval of* commercial products or services referenced herein.

Disposition

Destroy this report when it is no longer needed. Do not return it to the originator.

Unclassified

SECURITY CLASSIFICATION OF THIS PAGE (When Data Entered)

REPORT DOCUMENTATION PAGE

READ INSTRUCTIONS BEFORE COMPLETING FORM

(18) 1. REPORT NUMBER: DELET-TR-78-0563-1 (19) TR-78-0563-1

2. GOVT ACCESSION NO.

3. RECIPIENT'S CATALOG NUMBER

(6) 4. TITLE (and Subtitle): Lithium-Thionyl Chloride Battery.

5. TYPE OF REPORT & PERIOD COVERED: First Quarterly 10/1/78 to 12/31/78

6. PERFORMING ORG. REPORT NUMBER

(10) 7. AUTHOR(s): A. N. Dey, W. Bowden, J. Miller, P. Witalis

(15) 8. CONTRACT OR GRANT NUMBER(s): DAAB07-78-C-0563

9. PERFORMING ORGANIZATION NAME AND ADDRESS: P. R. Mallory & Co. Inc. Laboratory for Physical Science Burlington, Mass. 01803

215 325

(16) 10. PROGRAM ELEMENT, PROJECT, TASK AREA & WORK UNIT NUMBERS: 1L162705AH94 11-219 (17) 27

11. CONTROLLING OFFICE NAME AND ADDRESS: U. S. Army Electronics Technology & Device Lab. ERADCOM Attn: DELET-PR Ft. Monmouth, New Jersey 07703

(11) 12. REPORT DATE: April 1979

13. NUMBER OF PAGES: 57

14. MONITORING AGENCY NAME & ADDRESS (if different from Controlling Office)

15. SECURITY CLASS. (of this report): Unclassified

15a. DECLASSIFICATION/DOWNGRADING SCHEDULE

16. DISTRIBUTION STATEMENT (of this Report)

Approved for Public Release
Distribution Unlimited

(12) 70p.

17. DISTRIBUTION STATEMENT (of the abstract entered in Block 20, if different from Report)

(9) Quarterly rept. no. 1, 1 Oct-31 Dec 78,

18. SUPPLEMENTARY NOTES

19. KEY WORDS (Continue on reverse side if necessary and identify by block number)

Inorganic electrolyte battery, thionyl chloride, lithium, high rate D cell, high rate flat cylindrical cell, laser designator battery, cyclic voltammetry.

20. ABSTRACT (Continue on reverse side if necessary and identify by block number)

This report summarizes the activities carried out on Contract DAAB07-78-C-0563 during the period October 1, 1978 to December 31, 1978.

The objective of this program is to develop safe $Li/SOCl_2$ batteries for high rate U.S. Army applications such as man pack radios (BA5590) and GLLD laser designators.

During the first quarter, we have worked in the following three areas:

DD FORM 1 JAN 73 1473 EDITION OF 1 NOV 65 IS OBSOLETE

Unclassified

SECURITY CLASSIFICATION OF THIS PAGE (When Data Entered)

275 325

1. Improvement of the current capability of the spirally wound D cells.

2. Development of a 3 inch diameter flat cylindrical cell for the GLLD laser designator application.

3. Research on the $SOCl_2$ reduction mechanism.

The short circuit currents of the spirally wound D cells were increased from 20-30A to 100A corresponding to short circuit current densities of 200 mA/cm^2. This improvement was accomplished by improving the cathode current collector design.

The design and procurement of the parts and tooling for the fabrication of the 3 inch diameter flat cylindrical cell has been completed. In addition we evaluated the effect of cathode current collector design on the short circuit and the polarization characteristics of the disc shaped cathodes using a demountable flat cylindrical experimental cell. The maximum short circuit current densities obtained from these cathodes were similar to those obtained from the improved spirally wound cathodes in the D cells. We are now in the process of improving the fabrication methods for the flat cylindrical cell so that these can be made reproducibly. The electrical and safety testing of these cells will begin during the next quarter.

Cyclic voltammetry was used to investigate the electrochemical reduction of $SOCl_2$ in various supporting electrolytes which dissolve chloride salts thus avoiding any electrode passivation problem due to LiCl precipitation. It was established that although the Cl^- ion was formed immediately, reaction products such as S, SO_2 and S_2Cl_2 were not formed immediately upon reduction of $SOCl_2$. In addition, it was found that exhaustive electrolysis of $SOCl_2$ at a constant potential leads to the exhaustion of $SOCl_2$ but the latter was regenerated on warming the solution. These results may be relevant to the intrinsic safety of the system.

We plan to continue the above activities and to start the development of a spirally wound cylindrical cell for the GLLD laser designator application during the next quarter.

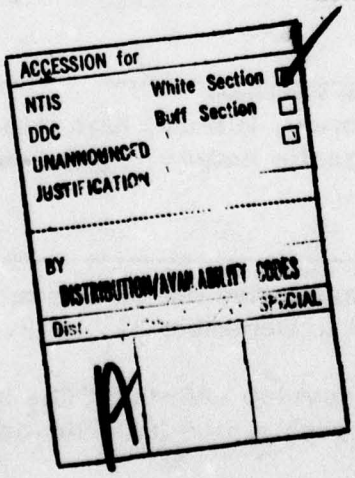

Table of Contents

List of Figures

List of Tables

I. Introduction

The $Li/SOCl_2$ inorganic electrolyte system (1-4) is the highest energy density system known to date. It consists of a Li anode, a carbon cathode and $SOCl_2$ which acts both as a solvent and as a cathode active material. The electrolyte salt that has been used most extensively is $LiAlCl_4$, but salts such as $Li_2B_{10}Cl_{10}$ (5) and $Li_2(OAlCl_3)_2$ (6) have also been used successfully in this system for improving the shelf life characteristics.

The main objective of this program is to develop high rate $Li/SOCl_2$ cells and batteries for various portable applications of the U. S. Army. The cells and batteries must deliver higher energy densities than are presently available and must be safe to handle under U. S. Army field conditions.

We carried out a detailed development (7) on the spirally-wound high rate D cells in order to establish their performance capabilities as well as to identify and correct the limitations in their performance and safety under various use and abuse conditions. Substantial progress was made to correct the cell limitations, and we found that the state-of-the-art spirally-wound D cells approach the high rate requirements of the various U. S. Army applications more closely than do any other cell design at the present time. Accordingly we have used this spirally-wound D cell as a starting point and have attempted to improve its rate capability in order to meet the requirements of two specific applications, viz. the BA5590 Battery for Man Pack Radio and the Battery for the GLLD Laser Designator.

In addition, we have begun the development of a 3 inch diameter flat cylindrical cell for the latter application. This cell has better heat dissipation characteristics than do the cylindrical D cells because of its higher outer surface area to volume ratio. We have plans to develop a 1.8 inch diameter cylindrical cell for the latter application as well which requires pulse currents

of 17.5A. This 1.8 inch diameter cell is expected to have roughly twice the current carrying capability of the D cells.

A parallel research effort has been initiated in order to gain an increased understanding of the cell discharge reactions, particularly with respect to the unstable intermediates. We believe that this knowledge will be useful in providing guidance for improving the safety of the system. The progress made in all the above areas during the first quarter of this program is described in this report.

II. Spirally Wound D Cell

The cross-sectional view of a typical spirally-wound hermetic D cell is shown in Fig. 1. We developed two types of spirally-wound cells, one for low rates having 10-15 inch long electrodes and 0.5M $LiAlCl_4$-$SOCl_2$ electrolyte, and the other for higher rates having 20 inch long electrodes and 1.0M $LiAlCl_4$-$SOCl_2$ electrolyte. The design details are available elsewhere (7, 8). The energy densities as a function of the discharge current for the two types of cells are shown in Fig. 2. Typical discharge curves of the high and the low rate cells are shown in Fig. 3 and 4 respectively. Note that the low rate cells are capable of delivering capacities of 18-19 A.Hr corresponding to energy densities of 20 WHr/in^3 and 300 WHr/lb and a $SOCl_2$ utilization of 95-98% based on the following cell reaction stoichiometry.

$$2Li + SOCl_2 \longrightarrow 2LiCl + SO \quad \ldots\ldots\ldots\ldots\ldots\ldots [1]$$

Therefore, this represents the upper limit of energy density available from this system and we do not anticipate any significant gain by additional effort to improve the cell further. The high rate cells, on the other hand, deliver maximum energy densities of only 13 WHr/in^3 and 190 WHr/lb although this energy density remains virtually constant up to 1.0A drain. The $SOCl_2$ utilization efficiency corresponding to the maximum energy density of the high rate cells was only 70-75%. The energy densities drop sharply above 2.0A. These energy density penalties at high rates stem from (a) lower operating voltages and (b) lower capacity (utilization efficiency). The former is dependent upon the electrical conductivity of the grid and the electrolyte and the latter is dependent upon the mass transfer (diffusion of active material) in the porous carbon cathode which is the capacity limiting electrode. Therefore, assuming that we use the electrolyte with the highest electrical conductivity, there are two major areas of work for improving the rate-capability of the cells:

1. Optimization of the cathode collector design, and
2. Optimization of the porous cathode structures.

We have determined the longitudinal reaction profile in the state-of-the-art cathodes by monitoring the LiCl content of the discharged cathodes at the various parts along its length starting from the tab onwards. The results for 2A discharge, at three different stages of discharge, are shown in Fig. 5. Note that at the early stages of discharge, (2.5 AHr and 5.4 AHr), most of the reaction occurs near the tab. This demonstrates that at 2A and high currents, the electrical conductivity of the cathode grid controls the current distribution. The higher the current, the greater the non-uniformity of the current distribution. Therefore, our first task was to optimize the current collector design of the cathode of the spirally-wound D cell.

A. Optimization of the Cathode Current Collector

For this study, we kept the cathode mix composition and the cathode fabrication process invariant in order to keep the porosity of the carbon cathodes identical for all the cathode collector designs. The carbon cathode consists of an expanded Ni grid covered with Shawinigan Black + 10% Teflon mixture on both sides of the grid. The selection of the above was made from the optimization of the carbon mixture and the carbon types, carried out earlier (9, 10). We chose to investigate two sizes of the cathodes, viz, 20" x 1.75" x 0.025" and 25" x 1.75" x 0.015". The various collector designs studied are discussed below.

1. One Tab on End Standard Design: This cathode design consists of one tab welded vertically at one end of the 20" x 1.75" cathode strip as shown in Fig. 6 (1). This is the standard design that has been used in all the D cells studied so far (7). The longitudinal reaction profiles shown in Fig. 5 refers to this design.

2. One Tab in Middle Design: In this design the one vertical tab is located at the center of the 20" x 1.75" electrode as shown in Fig. 6 (2).

3. Two Tab Design: In this design the two tabs are placed in such a manner that the farthest points from both the tabs are identical and are 5 inches away for the 20" x 1.75" cathode. A schematic view of the cathode design is shown in Fig. 6 (3). The total current is distributed evenly between the two tabs.

4. Horizontal Tab with Single Vertical Tab Design: In this design one horizontal tab is welded on one side of the cathode along its length and a vertical tab is welded at one end for connecting the cathode to the cell terminal as shown in Fig. 6 (4). In this design the maximum distance from the tab is the width of the cathode and as such the current collection should be most efficient.

5. Horizontal Tab with Double Vertical Tab Design: In this design, two vertical tabs, located 5 inches from either ends of the cathode, were used in addition to the horizontal tab as above. The schematic view is shown in Fig. 6 (5).

6. One Tab-Long Cathode Design: This design is identical to the design 1, above, except that the cathode is 25" long (Fig. 6 (6)) instead of 20" long.

7. Horizontal Tab-Long Cathode Design: This design (Fig. 6 (7)) is identical to the design 4, above, except that the cathode is 25" long.

8. Triple Tab-Long Cathode Design: In this design three tabs were used, one located at the center and the other two were located at either ends of the 25" long cathode. The schematic view is shown in Fig. 6 (8).

a. Experimental

Hermetic D cells were made by winding the cathode, Li anode and glass filter paper separator in Ni cans for evaluating the efficacy of the cathode on the rate capability of the cells. All the cells were filled with 1.8M $LiAlCl_4$-$SOCl_2$ electrolyte.

The tabs were 0.002" thick and 0.25" wide and were folded over the expanded Ni grid which was exposed by removing the carbon mix from the grid area where the tabs were welded. Thus each tab consists of a double layer of 0.002" Ni foil.

Some other specific construction details of the D cells with the various cathode designs are described below.

Design #1. Li anode dimension was 21" x 2" x 0.015"; one tab was attached at one end of the anode.

Design #2. Li anode was identical to design 1.

Design #3. Li anode was made by sandwiching expanded Ni current collector with a 0.25" wide tab welded horizontally lengthwise between two layers of 0.005" thick Li foil. Overall Li anode dimension was 21" x 2" x 0.010".

Design #4. Li anode was identical to design 1. The horizontal tab on the cathode was attached by welding two layers of the 0.25 inch wide tab on either side of the expanded Ni grid which was stripped of the carbon mix. The edge of the thin horizontal tab was very sharp and it cut through the separator to cause the cells to short during assembly. In order to prevent this, a thin Teflon film was folded over the horizontal tab of the cathode. This made the fabrication of these cells quite cumbersome.

Design #5. The Li anodes were similar to those of design 3 and the fabrication of these cells was as difficult as in design 4.

Design #6. The Li anode dimensions were 26" x 2" x 0.01", and it had one set of vertical tabs at one end of the anode as in design 1.

Design #7. The Li anode dimensions were 26" x 2" x 0.01" and it had expanded Ni current collector with 0.25" wide Ni tab welded horizontally, similar to that used in design 3. The cathode was covered with Teflon film over the horizontal and vertical tab areas.

Design #8. The Li anode was identical in construction to that of design 7. The construction of these cells was considerably easier than that of cells of design 7 because of the absence of the horizontal tab.

The polarization characteristics at currents below 17.5A and the short circuit currents at 25°C were measured for all the hermetic D cells made according to the above designs. The results will be used to select the promising cell designs for detailed performance evaluation according to the requirements of the BA5590 and the GLLD Laser Designator Batteries.

b. Results and Discussion

The electrical resistance of the 2" wide Li anode was calculated to be 0.113 and 0.169 miliohm/inch for 0.015" and 0.01" thick foils respectively, using the 8.6×10^{-6} ohm/cm as the resistivity of Li metal. The electrical resistance of two layers of the 0.25 inch wide and 0.002 inch thick Ni foil was calculated to be 2.677 miliohm/inch using 6.8×10^{-6} ohm/cm as the resistivity of Ni. The electrical resistance of the 1.75 inch wide expanded Ni was experimentally determined (Fig. 7) to be approximately 14.4 miliohm/inch. In Fig. 7 the electrical resistance at zero length corresponds to the resistance of the tab. Thus the cathode grid resistance was two orders of magnitude higher than the electrical resistance of the Li anode and as such the cathode current collector design becomes a controlling factor in the discharge of the cells at high rates. The Li anode current collector is unimportant insofar as the short circuit current and the current distribution at high currents are concerned but it is important insofar as the efficiency and uniformity of Li utilization are concerned.

The polarization characteristics of the hermetic D cells with 20" long cathodes of various current collector designs are shown in Fig. 8. Note that significant improvements in the polarization characteristics of the cells have been achieved over the standard cathode designs by designs #2 to #5. While the best performance was obtained with design #3, there was no significant difference between designs #2, #4 and #5. Note that design #2 is the simplest of all the designs and consists of a vertical tab located at the middle of the cathode strip as opposed to the end of the cathode strip. The cumbersome construction of cells with cathodes having horizontal tabs as in design #4 and #5 as well as the lack of any substantial improvement in performance over the simpler design #2, lead us to eliminate designs #4 and #5 from further consideration. The cells of design #3 consisting of two horizontal tabs performed best

among the cells with 20' long cathodes. Accordingly, both design #2 and #3 were selected for further studies.

The polarization characteristics of hermetic cells with 25" long cathodes are shown in Fig. 9. Note that significant improvements were realized with three tab designs over the single tab designs. The horizontal tabs (design 7) showed some improvement, but the difficulty in cell construction leads us to reject it from further consideration. The three tab design was found to be easier to construct and the cells performed the best. Therefore, we chose this design for further evaluation.

The short circuit currents of the hermetic D cells made with the various types of cathodes were measured through a 1 miliohm shunt. The maximum short circuit current of the various cells are shown in Table 1. The short circuit current densities were calculated using the apparent geometric areas of both sides of the cathodes. The short circuit current increased by a factor of three from design #1 to design #2 by placing the tab at the middle instead of at the end. Use of two tabs as in design #3 lead to a four-fold increase in the short circuit current (94A) over that of the standard design #1. The use of a horizontal tab (design #4) led to a modest increase in the short circuit current. This may be due to the reduction of the active area of the cathode by 14%. The use of the Teflon film may have aggravated the situation. The short circuit current of cathodes with both horizontal and two vertical tabs (design #5) was found to be similar to that of the cathodes with only two vertical tabs, thus indicating the lack of any significant contribution of the horizontal tabs. Therefore, designs #2 and #3 for the 20" long cathodes were chosen based on short circuit currents.

The short circuit currents of the cells with 25" long cathodes increased by a factor of two with a horizontal tab (design 7) and by a factor of three to 104A with a vertical three tab design. Again, the three tab design (design #8) was chosen for further studies.

The apparent short circuit current densities approached 200 mA/cm^2 for the better cathodes. The highest short circuit current densities were obtained with designs #3 and #5. The maximum distance from the tab was 5"

for design #3 and 1.5" for design #5 corresponding to total maximum resistances of 72 miliohm and 21.6 miliohm respectively. The impedance of Li and the tabs are negligibly small compared to the above values and since the above impedances are in series to make up the total cell impedance, further improvements of the short circuit current may be possible by reducing the resistance of the cathode current collector even further.

c. Conclusions

An analysis of the impedance of the various cell components and an analysis of the longitudinal cathode reaction profiles showed that the impedance of the cathode current collector is a significant contributor to the cell impedance leading to non-uniform current distribution and low current carrying capability.

Eight different cathode current collector designs were investigated using hermetic D cells with wound electrode assembly. Based on the polarization characteristics and the short circuit currents, three designs were found to be promising and were selected for further evaluation.

Short circuit currents approaching 100A and current densities of 200 mA/cm^2 were realized by the above approach.

III. Flat Cylindrical Cell

The safety of the $Li/SOCl_2$ cells was shown (7, 11) to depend on the internal temperature of the cells. DTA studies of the cell constituents showed that Li + S exothermic reactions which occur at temperatures of approximately 150°C may be responsible for the thermal runaway of the $Li/SOCl_2$ batteries. Therefore, it is important that the temperatures of the cells be kept below 150°C under all conditions of use and abuse. For low rate applications the safety of the cells was successfully achieved by controlling the heat generation of the cells by lowering their intrinsic rate capability. However, for high rate applications, such as the GLLD laser designator which requires pulse currents of 17.5A at 24 volts involving a power drain of 420 watts, the heat generation of the cells cannot be easily controlled. Therefore, in order to maintain the internal cell temperature below 150°C, the heat dissipation of the cells must be enhanced and cell configurations with a maximum surface area to volume ratio are preferable. Considering only the cylindrical shape, in view of its advantage in terms of containing high internal pressures with minimal distortion, the surface to volume ratio, R is expressed as

$$R = \frac{2\pi r^2 + 2\pi rl}{\pi r^2 l} = \frac{2}{l} + \frac{2}{r} \quad \ldots\ldots\ldots\ldots\ldots\ldots [2]$$

where r is the radius and the l is the length of the cylinder.

The surface/volume ratio can be increased either by decreasing the length of the cylinder while increasing the radius to maintain the internal volume, or by decreasing the radius of the cell and correspondingly increasing the length. Considering the difficulties involved in the construction of narrow cylindrical cells, we opted in favor of the former shape, viz., the flat cylindrical cell.

The electrode designs chosen for this cell consisted of stacked circular discs instead of the commonly used spirally wound electrodes. We optimized the current collector design of the carbon cathode by measuring the polarization characteristics of the circular disc shaped cathodes using a demountable flat

cylindrical experimental cell. We also made progress in the design and the procurement of the tools and the parts needed to construct the hermetic flat cells. The experimental details and the results are described here.

A. Experimental

a. Demountable Flat Cylindrical Cell

We designed and built a flat cylindrical cell which can be easily assembled and disassembled for the purpose of evaluating the effect of the current collector design in the performance of the disc shaped carbon cathodes. The cell is made of two thick stainless steel plates which act as heat sinks to prevent any significant temperature rise in the cell which may affect the polarization measurements. The disc shaped Li anode and carbon cathode are welded on the stainless steel plates by means of tabs of various designs. The schematic view of the experimental cell is shown in Fig. 10. The two plates are insulated by means of viton rubber gaskets and the sealing of the cell was accomplished by compressing the plates with polypropylene nuts and bolts. The cell contained an Li reference electrode connected to a nickel tab which is placed between the two layers of the viton rubber gaskets. The two stainless steel plates acted as cell terminals. The cell was filled with 1.8M $LiAlCl_4$-$SOCl_2$ electrolyte through an electrolyte fill port located in one of the plates.

The disc electrodes were 2.8 inch in diameter. The Li anode was made by punching out 2.8 inch discs of 15 mil thick Li and pressing it on the expanded Ni current collector which was welded to one of the stainless steel plates.

The carbon cathode was similar in composition and thickness (0.025 in) as used in D size cells and comprised porous carbon on expanded Ni current collector. Carbon cathodes were made by punching out 2.8 inch diameter discs from a sheet of carbon cathode. The details of the various current collector designs are shown in Fig. 11. Altogether eight different designs were studied. The details of the various current collector designs are described below.

Design #1. In this design the expanded Ni grid of the carbon was welded to the stainless steel plate at four different spots as shown in Fig. 11 (1). There was no separate tab for the current collection. There was no significant reduction of the active carbon area in this design, since weld areas were very small and the amount of carbon removed from the grid was negligible.

Design #2. In this design two layers of 0.20 inch wide Ni ring was welded all around the carbon cathode. The thickness of each layer of the ring was 0.01 inch. The Ni ring was then welded to the stainless steel block at four different spots as shown in Fig. 11 (2), without any tab. This design leads to a reduction of the active carbon area of approximately 27%.

Design #3. This design was identical to design #2 in all respects except that the Ni ring was 0.005 inch thick.

Design #4. In this design, the cathode with the metal ring as in design #2, was welded to the stainless steel block by means of two layers of 0.25 inch wide, 0.002 inch thick Ni tab. The length of the tab was approximately 0.25 inch. The cathode was otherwise insulated from the stainless steel block by a layer of separator.

Design #5. In this design two layers of 0.25 inch wide Ni tab was connected to one edge of the cathode disc and then welded to the stainless steel block of the cell. There was virtually no loss of the active cathode area by this design. The cathode was otherwise insulated from the block by means of a layer of glass filter paper separator.

Design #6. In this design, two layers of 0.25 inch wide Ni tab were welded from the center to the edge of the cathode disc, as shown in Fig. 11 (6). This tab was then welded to the stainless steel block. There was also a layer of separator between the cathode and the cell block. The reduction in active cathode area was approximately 9%.

Design #7. In this design two layers of 0.125 inch wide tab were welded across the diameter of the cathode disc as shown in Fig. 11 (7). The cathode was also separated from the block as before. The reduction in active area as a result of the tab was approximately 6%.

Design #8. In this design two 0.125 inch wide tabs (two layers) were welded at 90 degrees along the diameter of the cathode disc as shown

in Fig. 11 (8) . The two tabs were welded to the stainless steel cell block and the cathode was separated from the block by glass filter paper separator. The reduction of the active area was approximately 12%.

The cell was made with the above cathodes and Li anode with glass filter paper separator. Only one side of the electrodes was used. Both the short circuit current and the polarization characteristics were measured. During the polarization measurements, both the cell voltage and the cathode potential against the Li reference electrode were measured. All the measurements were made at room temperature. The wall temperature of the cells were monitored during the above measurements, and it remained constant.

b. Flat Cylindrical Cell Design

The overall dimensions of the flat cylindrical cell are: OD: 3.00 inch, Ht: 0.50". The design of the flat cell can is shown in Fig. 12. The can was made of 304 stainless steel which is compatible with the system.

The flat cell cover design is shown in Fig. 13. It contains a glass-to-metal seal terminal and an electrolyte fill port. The material of the cover was also 304 stainless steel.

The cross sectional view of the cell with the disc electrode stack is shown in Fig. 14.

The procurement of cans and covers was completed. The tooling needed to make the cover assembly with G/M seal is in the process of being perfected. We made several experimental runs.

The tooling for punching out the electrodes has been developed for the initial electrode studies.

The development of appropriate tooling for welding the cell top has also been completed.

We made some flat cylindrical cells in order to check out the assembly and the welding steps. A photograph of a finished cell is shown in Fig. 15. The testing of these flat cells will begin when the assembly steps have been perfected.

B. Results and Discussion

a. Effect of Cathode Current Collector Design on the Polarization Characteristics of the Experimental Flat Cells

The results of the cathode and the cell polarization data are provided in Table 2. The difference between the cathode and the cell polarization represents the internal cell impedance which varied from 0.01 to 0.1 ohm from cell to cell as well as from current to current. This relatively high cell impedance stems from the relatively large space between the anode and the cathode as necessitated by the particular stainless steel block cell design. For the purpose of comparing the effect of the various current collector designs we chose to use the cathode polarization data as measured against the Li reference electrode.

The cathode polarization characteristics of the eight different types of current collector designs are shown in Fig. 16 and 17.

The results of the first four designs are shown in Fig. 16. Note that the polarization characteristics of the four types of cathodes are virtually identical in spite of the fact that the cathodes of design 2, 3 and 4 has 27% less active area than the cathodes of design 1. This demonstrates that the detrimental effects of lower electrode area has been successfully compensated by the beneficial effect of the improved current collection as in design 2, 3 and 4. The results of the designs 5, 6, 7 and 8, as shown in Fig. 7 also show the lack of significant differences in the polarization characteristics of the various cathode designs. Therefore, we conclude that for the 2.8 inch diameter disc cathodes, the current collector design does not have any dramatic effect on the polarization characteristics of the cathodes. The designs which are most convenient for the construction of electrode stack are 5, 6 and 7.

b. Effect of Current Collector Designs on the Short Circuit Currents

The short circuit currents of the experimental flat cells with the cathodes of eight different designs are shown in Table 3. The lowest short circuit was obtained with design #5 having one tab connected at one point at the edge of the disc, indicating the poor current collection of this design. The higher short circuit currents of the other designs indicate the relative compensatory effects between the mass transport and the current collection. Based on the short circuit current, the designs 6 and 7 emerge as the preferable designs for the high rate cathodes. The highest short circuit current density realized from these cathode designs was 200-230 mA/cm^2, very similar to that realized from the spirally wound D cells indicating the adequacy of the current collection.

C. Conclusions

The effect of the cathode current collector design on the polarization and the short circuit current of the flat cells did not appear to be as dramatic as in the case of spirally wound D cells of the eight different current collector designs investigated. Two were chosen for further evaluation in the hermetic flat cylindrical cell. These designs have a current collector tab located along the radius and along the diameter of the circular disc shaped carbon cathode. These two designs combine the least reduction in the active carbon area and an efficient current collection for the 2.8 inch diameter cathode. The maximum short circuit current densities were 200-230 mA/cm^2, very similar to that realized in spirally wound D cells having improved cathode current collectors.

IV. Cyclic Voltammetric Studies on the $SOCl_2$ Reduction Mechanism

Calorimetric (12) and DTA studies (7, 11) of Li/$SOCl_2$ D cells showed that chemical reactions continue to occur liberating heat after the discharge of the cell. Since these reactions do not occur in an undischarged cell, it is reasonable to assume that the reduction products of $SOCl_2$ are responsible, at least in part, for these spontaneous exothermal reactions. The reported spontaneous explosions of partially discharged Li/$SOCl_2$ cell on casual storage may also be initiated by the above unknown reactions involving the $SOCl_2$ reduction intermediates. Thus, knowledge regarding the nature of the unstable intermediates of $SOCl_2$ reduction may be useful as a guide for the improvement of the safety of the Li/$SOCl_2$ cells. We postulated (9, 13) the overall cell reaction to be

$$SOCl_2 + 2Li \longrightarrow SO + 2LiCl \quad \text{.....} \quad [3]$$

where SO may dimerize and then decompose to S and SO_2 or may form polymers. Although there is substantial evidence (5, 14) in favor of cell stoichiometry [3] and the quantitative formation of LiCl and qualitative formation of S and SO_2, very little is known regarding the intermediates formed during the discharge of $SOCl_2$. Attempts to use cyclic voltammetry (15, 16) in neat $SOCl_2$-$LiAlCl_4$ solutions to study the discharge reaction were complicated by the electrode passivation due to the precipitation of LiCl which is insoluble in $SOCl_2$. We have circumvented this electrode passivation problem by using a supporting electrolyte consisting of tetrabutylammonium hexafluorophosphate in organic solvents such as dimethyl formamide (DMF) and acetonitrile (AN) for studying the $SOCl_2$ reduction. The electrode passivation was absent in the above solutions since both tetrabutylammonium chloride and S are soluble in DMF and AN. We carried out both cyclic voltammetry and coulometry in the above electrolytes. The results are reported here.

A. Experimental

Electrochemical experiments were performed using a PAR 173 potentiostat and PAR 175 function generator with associated ancillary equipment.

Data were collected using conventional x-y and strip chart recorders. Platinum working electrodes were pretreated by chromic acid followed by a wash with distilled water and air drying. Experimental solutions were routinely degassed with argon before the substrates were added. A silver chloride coated silver wire was used as a reference electrode. This electrode has a potential of 3.30V vs. Li in PF_6^--DMF solutions.

Experiments were performed in cells of conventional design. Coulometric experiments were carried out in a two compartment H-cell using a glass frit to prevent passage of material from the working and auxiliary electrode compartments.

Organic solvents were either Burdick & Jackson "Distilled in Glass" DMF, and CH_2Cl_2 or Eastman Spectro Grade acetonitrile. Supporting electrolyte was prepared by metathesis of tetrabutylammonium chloride (TBACl) and lithium hexafluorophosphate in acetone/water and purified by multiple re-crystallizations in hot ethanol.

B. Results and Discussion

The electrochemical characteristics of some of the impurities and proposed reduction products of $SOCl_2$ were examined by cyclic voltammetry in the organic supporting electrolyte solutions. In particular, sulfur, sulfur monchloride, and sulfur dioxide are materials of interest, while chloride ion is generally accepted as a reduction product.

a. Chloride

A cyclic voltammogram on Pt electrode in $TBAPF_6$ in AN is shown in Fig. 18 which demonstrates the clean background. A suitable chloride source was found in tetramethylammonium chloride (TMACl) which is both soluble and ionized in acetonitrile solution. A cyclic voltammogram obtained with a platinum wire electrode of a solution of TMACl and $TBAPF_6$ in AN is shown in Fig. 19. The oxidation of free chloride to chlorine and the associated reduction to chloride are clearly located about 1.1V positive of the reference potential.

b. Sulfur Dioxide

The electrochemical reduction of sulfur dioxide is itself of considerable practical importance and reasonably stable solutions of sulfur dioxide in organic solvents are easily obtained. The reduction of SO_2 in DMF, acetonitrile and methylene chloride has been examined. In acetonitrile, SO_2 is reduced in a diffusion controlled process at E 1/2 - 1.15V vs. the silver reference as shown in Fig. 20. The oxidation wave with E_p near +0.35V is much diminished at lower sweep rates and represents the oxidation of a product of the SO_2 reduction, viz. $S_2O_4^{2-}$ according to the reaction

$$SO_2 + e \longrightarrow SO_2^- \quad \ldots\ldots\ldots\ldots\ldots\ldots\ldots \quad [4]$$

$$2(SO_2)^- \longrightarrow S_2O_4^{2-} \quad \ldots\ldots\ldots\ldots\ldots\ldots\ldots \quad [5]$$

Even at the relatively high sweep rate of 1V/sec there is little evidence for any other oxidation peaks corresponding to the oxidation of species such as SO_2^-. A similar voltammogram of SO_2 in dimethylformamide solution is shown in Fig. 21 under similar circumstances. Once more E1/2 is near -1.15V and there is a kinetic oxidation wave due to SO_2 reduction products, but there is also a small wave near -0.13V which is due to a new product species. Finally, SO_2 was also examined in methylene chloride solution, where two oxidation peaks corresponding to the oxidation of SO_2^- and $S_2O_4^{2-}$ are more apparent, as shown in Fig. 22. In general the initial reduction behavior of the SO_2 in organic solvents was quite consistent, with the established mechanisms (20) but the oxidation of the reduction products was substantially affected by the solvent, probably due to varying degrees of saturation of the two reduced species, SO_2^- and $S_2O_4^{2-}$.

c. Sulfur

The cyclic voltammetry of sulfur was examined in dimethylformamide and methylene chloride because of the difficulty of dissolving sulfur in acetonitrile. In both methylene chloride and DMF, the reduction of sulfur is a rather complex phenomenon. The reduction of sulfur in CH_2Cl_2 as shown in Fig. 23, consists of two successive reduction waves whose relative heights are

sweep rate dependent (as V increases the second wave becomes less prominent) at ca. -1.1V and -1.5V with an oxidation near -0.2V which is also sweep rate dependent and becomes more prominent as the sweep rate increases. Both of these reduction processes appear to be quite irreversible. The reduction of sulfur in DMF, as shown in Fig. 24 again consists of two irreversible, but more widely spaced waves near -0.6V and -1.15V. The shape of this second reduction wave is dependent on sweep rate. Finally there is an oxidation wave, also irreversible at +0.25V. The species responsible for this oxidation has been shown by other voltammograms to be the product of the first reduction wave. The height of this oxidation wave is also a function of the sweep rate and becomes much more obvious at high sweep rates. In acetonitrile the cyclic voltammogram for sulfur is somewhat similar to that for DMF, although the second wave is much less well defined and the oxidation wave is near 0V.

d. Mixture of Sulfur and Sulfur Dioxide

Since both S and SO_2 are known to form in the cell, the cyclic voltammogram of a mixture of S with trace amounts of SO_2 in $TBAPF_6$-DMF electrolyte was obtained, and, as shown in Fig. 25(a), it contained only the two peaks corresponding to the reduction of S. Cyclic voltammograms of the same solution with slightly higher concentrations of SO_2, as shown in Fig. 25(b), contain three reduction peaks, the middle one represents the SO_2 reduction. There was no noticeable interaction between S and SO_2 that could be detected by the cyclic voltammetry.

e. Sulfur Monochloride

In contrast to the other products examined, S_2Cl_2 showed a complicated electrochemical behavior in organic solvents. As shown in Fig. 26, the voltammogram of S_2Cl_2 in acetonitrile is dominated by an adsorption wave near -1.15V. This wave is followed by an apparently reversible reduction near -1.75V. On the return sweep we see peculiar behavior suggesting adsorption of S_2Cl_2 or its products on the electrode surface. At $\sim$ +1.1V we see the oxidation of chloride generated during the reduction of S_2Cl_2.

f. Thionyl Chloride

A cyclic voltammogram for 50μl $SOCl_2$ in approximately 75 ml DMF with 0.1M $N(C_4H_9)_4 PF_6$ at a platinum wire electrode is presented in Fig. 27(a). The reduction of thionyl chloride shows two successive reduction waves with $E_{p/2}$ at -0.20V for the first wave, (17) with a peak potential which is sweep rate dependent, but near -0.37V, while the peak potential for the second reduction is near -0.65V. In addition to these reduction processes, there is an irreversible and broad oxidation on the return sweep near 0.0V. This oxidation wave is absent at lower sweep rates and more prominent at higher sweep rates of 200 mV/sec or more. The small reduction wave near -1.25V is present in the background and presumably due to a trace impurity in the DMF. Both of the reduction peaks due to thionyl chloride are due to diffusion controlled processes as shown by the linear relationship of the peak cathodic current i_{pc} and $\sqrt{V}$, where V is the sweep rate, as shown in Fig. 28. Under similar circumstances an adsorption controlled process would show i_{pc} linear with V and a kinetic controlled process is not a simple function of V (17).

This solution of DMF and thionyl chloride is sufficiently stable that an exhaustive electrolysis of the thionyl chloride can be performed at a platinum foil electrode. It is somewhat difficult to get completely reproducible n values from coulometry because of the closely spaced second reduction wave, but reduction at -0.25V gives an apparent n of 1.71-1.9 e per $SOCl_2$. A cyclic voltammogram of this reduced $SOCl_2$ solution is shown in Fig. 27(b). This reduced product is characterized by a reduction wave near -0.63V with little clear evidence for any oxidation processes. If this reduced solution is either allowed to stand or is slightly warmed with a water bath, some thionyl chloride is regenerated, as shown in Fig. 27(c). If this material is then further reduced at -0.25V, n is 2.04 or very nearly 2.0, while a shoulder appears near -0.9V.

The electrochemical behavior of sulfur, sulfur dioxide and sulfur monochloride and that of the reduced $SOCl_2$ solution lead to the conclusion that none of these three materials are immediately formed in the

reduction of thionyl chloride in DMF. We have observed identical reduced $SOCl_2$ products in a variety of solutions which enable us to rule out any reaction of solvent with $SOCl_2$ as the source of this behavior.

These findings suggest that the reduction of thionyl chloride is a more complex process than originally thought. A possible reaction scheme which is consistent with our experimental evidence involves an initial one electron reduction of $SOCl_2$ with expulsion of a chloride ion [6] which then undergoes some rapid chemical process such as shown in [7] and [8].

$$SOCl_2 + e \longrightarrow SOCl + Cl^- \quad [6]$$

$$SOCl + SOCl \longrightarrow (SOCl)_2 \quad [7]$$

$$(SOCl)_2 \longrightarrow SOCl_2 + SO \quad [8]$$

The highly reactive species SO may dimerize, disproportionate and then decompose to S + SO_2 or form polysulfur oxide (18) according to the reactions

$$2SO \longrightarrow (SO)_2 \quad [9]$$

$$(SO)_2 + SO \longrightarrow S_2O + SO_2 \quad [10]$$

$$2S_2O \longrightarrow SO_2 + S \quad [11]$$

$$m\ S_2O \longrightarrow (S_nO)_x + SO_2,\ n > 2 \quad [12]$$

or form some complex with excess $SOCl_2$ [13] which would remove $SOCl_2$ from solution until the complex is destroyed. The product of reaction [13] is stoichiometrically equivalent to the $(SOCl)_2$ dimer in [7].

$$SO + SOCl_2 \longrightarrow SO \cdot SOCl_2 \quad [13]$$

The polysulfur oxides may decompose to yield S and SO_2 which are thought to be the final electrolysis products. Other observations such as exothermic reactions in partially discharged cells (12) and delayed increase in gas pressure in discharged $SOCl_2$ cells (19) can also be explained in terms of this reaction scheme. These results may have some relevance to the chemical reactions in $SOCl_2$ cells and their subsequent safety.

C. Conclusions

We have obtained experimental evidence showing that the reduction of $SOCl_2$ does not lead to the immediate formation of S, SO_2 or S_2Cl_2. The intermediates formed are either sufficiently stable by themselves or they combine with $SOCl_2$ to form a relatively stable species. The most interesting finding is that after a constant potential electrolysis there is evidence for the regeneration of $SOCl_2$ on standing or warming of the solution. The observed spontaneous heat evolution (12) of a discharged cell may be explained in part by such a reaction. Although we do not have any direct evidence for the formation of SOCl and SO as yet, all our results so far are consistent with the hypothesis of their formation as intermediates in $SOCl_2$ reduction.

V. Conclusions and Future Work

The current carrying capability of the spirally wound D cells was improved substantially by improving the current collector of the cathode. Short circuit currents of 100A and short circuit current densities of 200 mA/cm^2 were realized by the above approach.

The development of a 3 inch diameter flat cylindrical cell for the GLLD laser designator application has proceeded on schedule. The current collector design of the disc shaped cathodes were optimized and short circuit current densities in excess of 200 mA/cm^2 were realized. We have made some experimental flat cylinder cells, and are now in the process of developing fabrication methods for them.

We have gained additional insight into the electrochemical reduction of $SOCl_2$ particularly into the pseudo stable intermediates and their possible effects on the cell chemistry. We have used only cyclic voltammetry so far but plan to augment these studies with other techniques in the future in an attempt to obtain direct evidence on the chemical nature of the reaction intermediates.

During the next quarter we plan to begin work on the development of the 1.8 inch diameter spirally wound cell for the GLLD laser designator application, in addition to continuing the above-mentioned activities that have already been initiated.

VI. References

1. W. K. Behl, J. A. Cristopulos, M. Ramirez and S. Gilman, J. Electrochem. Soc., 120, 1619 (1973).
2. J. J. Auborn, K. W. French, S. I. Lieberman, V. K. Shah and A. Heller, ibid, 120, 1613 (1973).
3. D. L. Maricle et al, U.S. Pat. 3, 567, 515 (1971); G. E. Blomgren and M. L. Kornenberg, German Pat. 2, 262, 256 (1973).
4. A. N. Dey and C. R. Schlaikjer, Proc. 26th Power Sources Symposium, Atlantic City, April 1974.
5. C. R. Schlaikjer, U.S. Pat. 4,020, 240 (1977), Proc. 28th Power Sources Symposium, Atlantic City, June 1978.
6. J. P. Gabano and P. Lenfant, Abstract No. 27, Electrochemical Society Meeting, Pittsburg, PA., Oct. 1978.
7. A. N. Dey, "Sealed Primary Lithium Inorganic Electrolyte Cell" Final Report, DELET-TR-74-0109-F, P. R. Mallory & Co., Inc., July 1978.
8. A. N. Dey and P. Bro., Proc. Brighton Power Sources Symposium (1976), p. 508.
9. A. N. Dey, J. Electrochem. Soc., 123, 1262 (1976).
10. A. N. Dey, J. Electrochem. Soc., (Communicated).
11. A. N. Dey, Proc. 28th Power Sources Symposium, Atlantic City, June 1978.
12. P. Bro, J. Electrochem. Soc., 125, 674 (1978).
13. A. N. Dey, Thin Solid Films, 43, 131 (1977).
14. D. R. Cogley and M. J. Turchan, "Lithium-Inorganic Electrolyte Batteries," Second Quarterly Report; ECOM-74-0030; AD 779477 EIC Inc., May 1974.
15. W. K. Behl, in "Proceedings of the 27th Power Sources Symposium," Atlantic City, N.J., June 1976.
16. G. E. Blomgren, V.Z. Leger, M. L. Kronenberg, T. Kalnoki-Kis and R. J. Brodd, in "Proceedings 11th International Power Sources Symposium," Brighton, England, 1978.
17. R. N. Adams "Electrochemistry at Solid Electrodes," Dekker (1969).
18. P. W. Schenk and R. Steudel, Angew. Chem. Internat. Edit. 4, 402 (1965).

19. M. Domeniconi, K. Klinedinst, N. Marincic, C. Schlaikjer, R. Staniewicz and L. Swette, "Inorganic Electrolytes," Office of Naval Research; Interim Report, Contract #N00014-76-C-0524; GTE Laboratories; Jan. 1976 to Oct. 1977.

20. R. P. Martin, Thesis "The Electrochemical Reduction of Sulfur Dioxide and of Elemental Sulfur in Nonaqueous Solvents," University of California, March 1973.

VII. Acknowledgement

Helpful suggestions from Dr. Sol Gilman and Dr. Per Bro and experimental assistance of Robin Granelli are gratefully acknowledged.

TABLE 1

Short-Circuit Currents of Hermetic D Cells with Various Cathode Designs

No.	Cathode Designs	Maximum Short Circuit Current (A)	Maximum Short Circuit Current Density (mA/cm^2)
1.	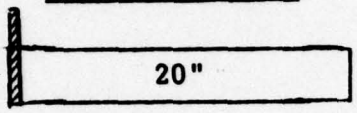	24	53
2.	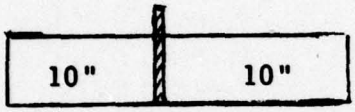	76	168
3.	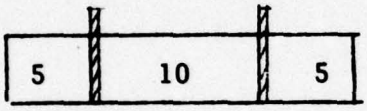	94	208
4.	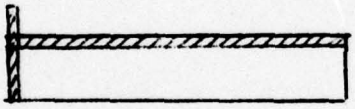	58	128
5.	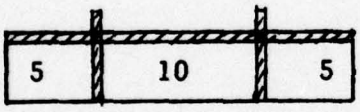	98	217
6.	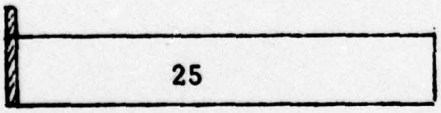	35	62
7.	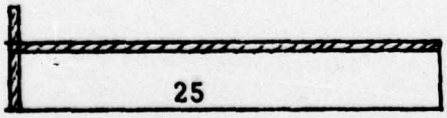	65	115
8.	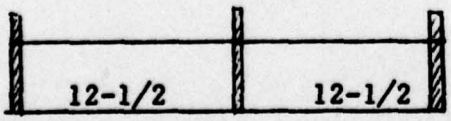	104	184

TABLE 2

Polarization Characteristics of the Flat Cells and the Circular Cathodes having Various Current Collector Designs

Current (A)	Design 1 		Design 2  (10)		Design 3  (5)		Design 4 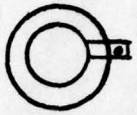		Design 5 		Design 6 		Design 7 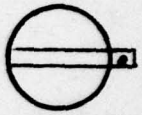		Design 8 	
	Cell Volt	Cath. Pot	Cell Volt	Cath. Pot	Cell Volt	Cath. Pot	Cell Volt	Cath. Pot	Cell Volt	Cath. Pot	Cell Volt	Cath. Pot	Cell Volt	Cath. Pot*	Cell Volt	Cath. Pot
0.1	3.39	3.40	3.30	3.40	3.33	3.36	3.35	3.38	3.37	3.39	3.33	3.38	3.35	3.40	3.34	3.37
0.3	3.20	3.27	3.15	3.28	3.15	3.21	3.19	3.23	3.18	3.23	3.18	3.26	3.22	3.30	3.16	3.22
0.5	3.10	3.15	-	-	-	-	-	-	-	-	-	-	3.14	3.16	3.06	3.14
1.0	2.80	2.87	2.80	2.96	2.70	2.89	2.85	2.91	2.80	2.90	2.84	2.87	2.96	2.99	2.81	2.94
2.0	2.35	2.41	2.35	2.59	2.30	2.50	-	-	-	-	2.50	2.55	2.69	2.74	-	-
3.0	1.95	2.10	-	-	-	-	-	-	-	-	-	-	-	-	-	-

* Projected Values; the Reference Electrode was Disconnected.

TABLE 3

Short-Circuit Currents of the Experimental Flat Cylindrical Cells with Various Cathode Designs

	Cathode Current Collector Design	Short Circuit Current (A)	Short Circuit Current Densities (mA/cm^2)
1.		7.0	176
2.	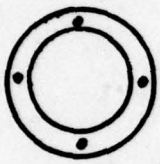 (10 mil)	8.0	201
3.	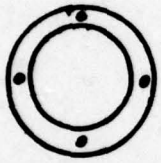 (5 mil)	7.4	186
4.	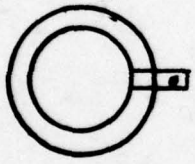	8.6	216
5.	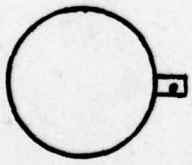	6.2	156
6.	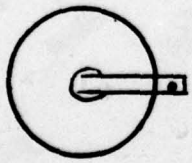	9.2	231
7.	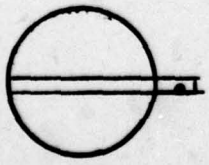	8.8	221
8.	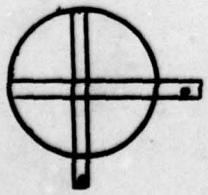	7.2	181

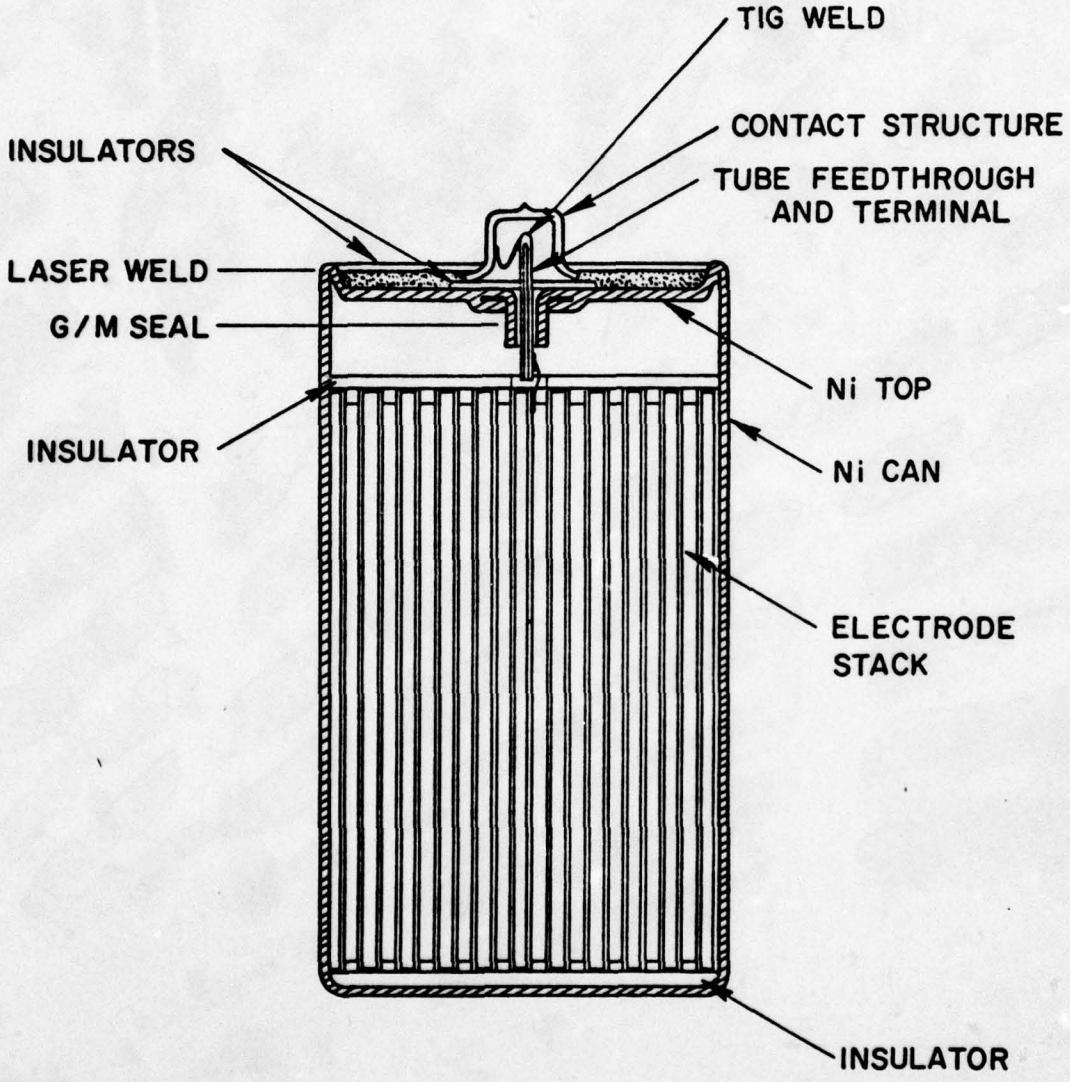

Fig. 1. Cross-Sectional view of the hermetic $Li/SOCl_2$ D cell.

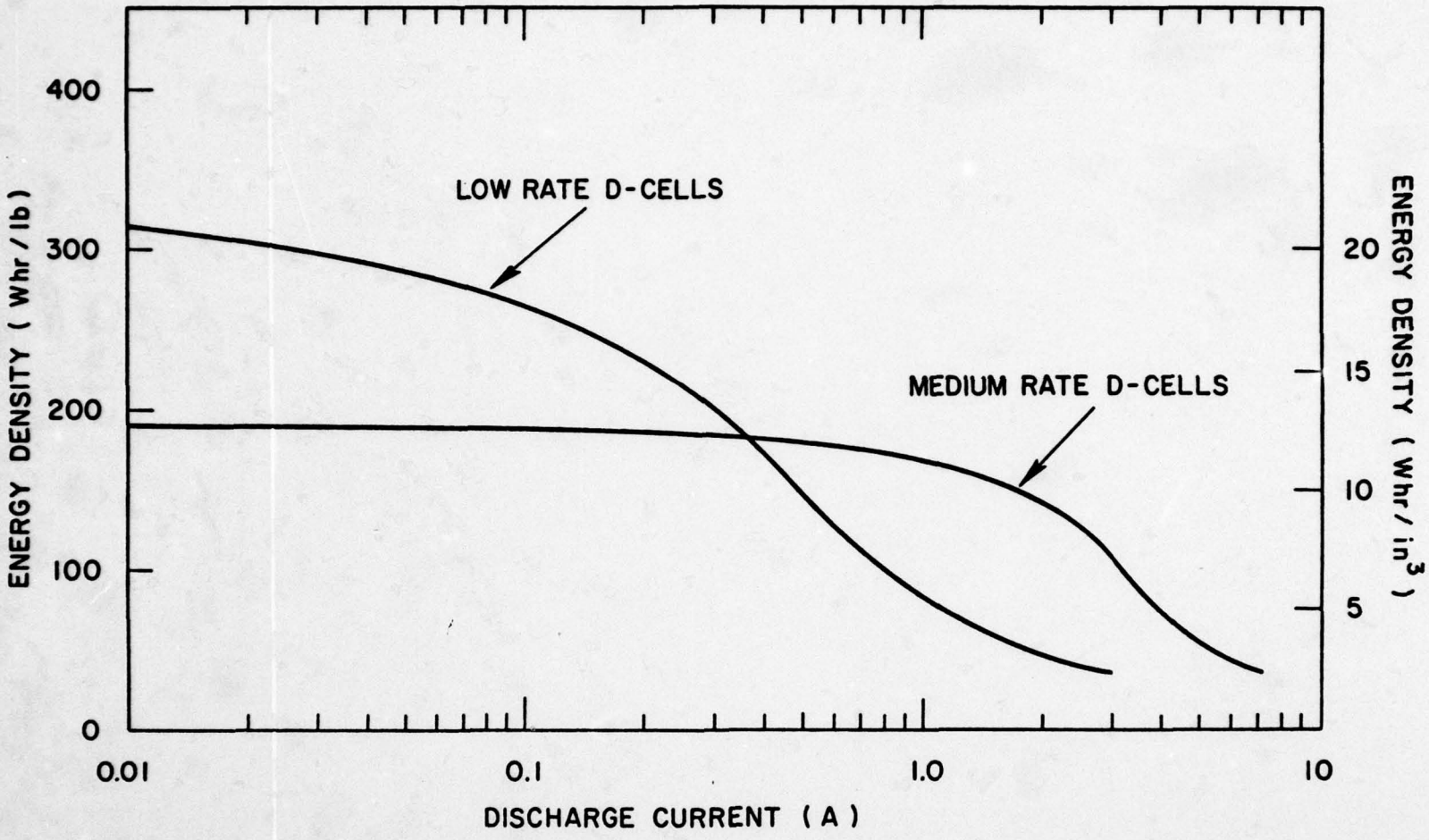

Fig. 2. Energy density-rate curves of the high rate and the low rate Li/$SOCl_2$ D cell.

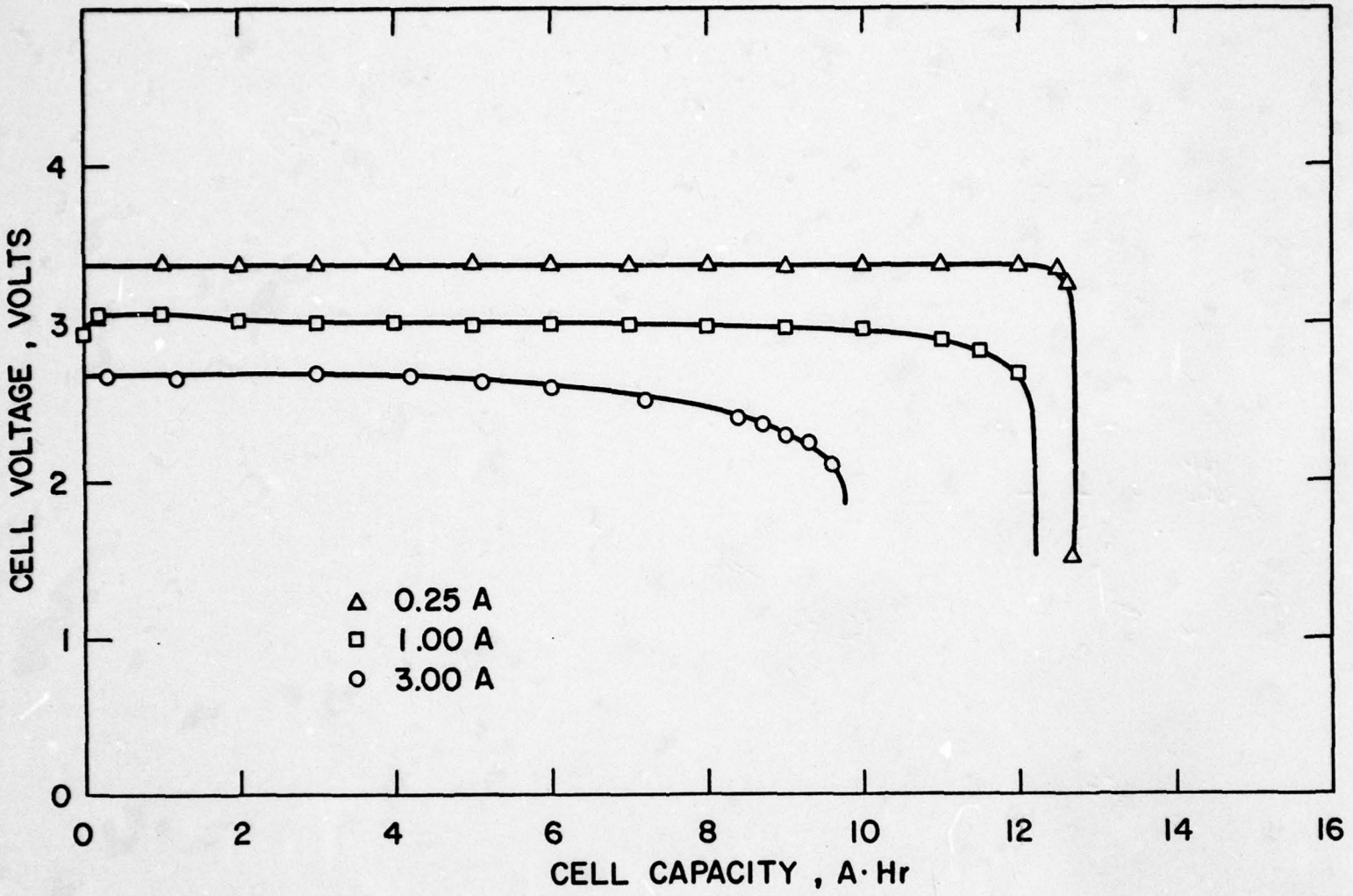

Fig. 3. Discharge characteristics of high rate Li/$SOCl_2$ D cells at constant currents of 0.25, 1.0 and 3.0A at 25°C.

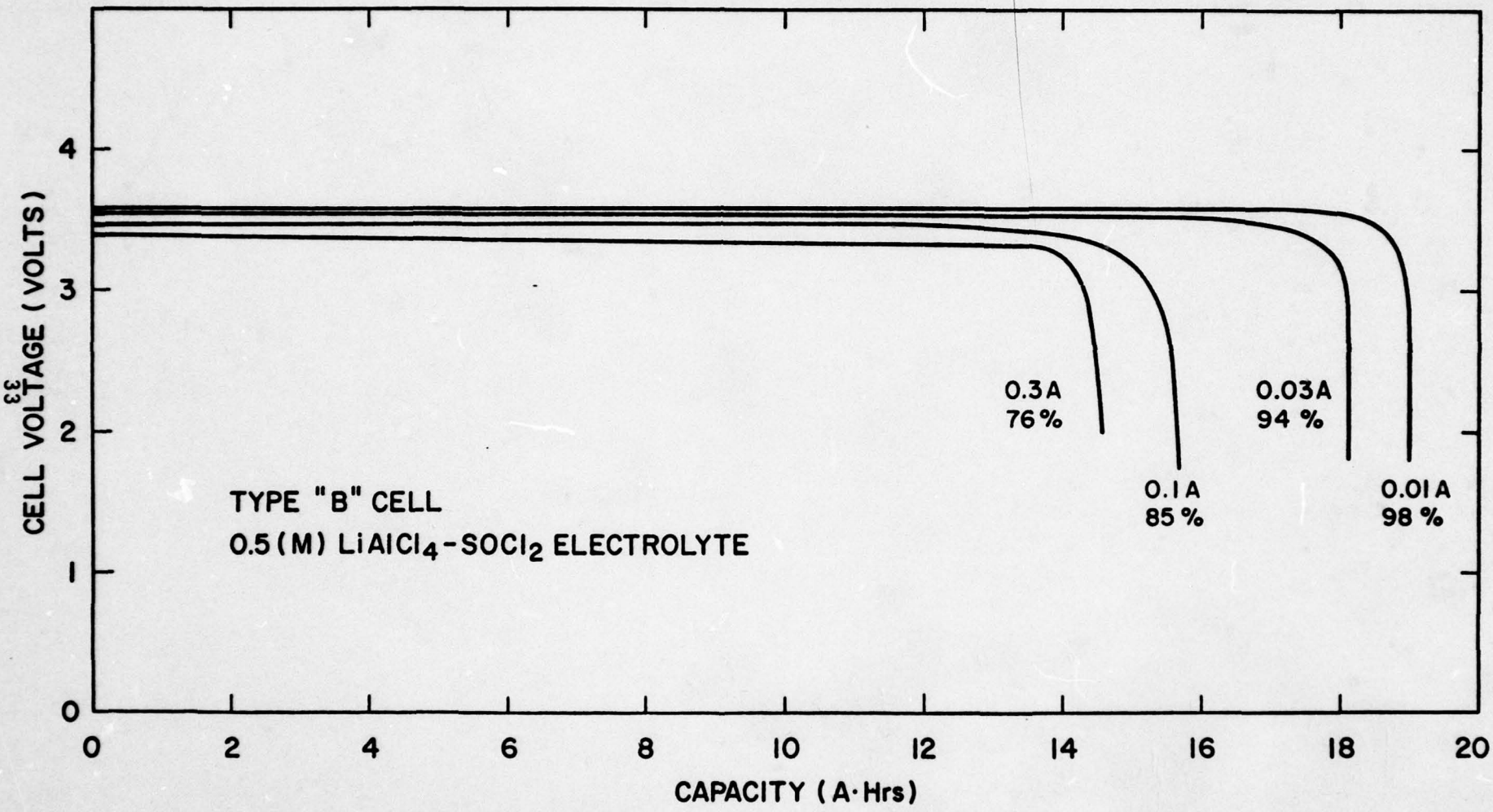

Fig. 4. Discharge characteristics of low rate Li/$SOCl_2$ D cells at constant currents of 0.01, 0.03, 0.1 and 0.3A at 25°C.

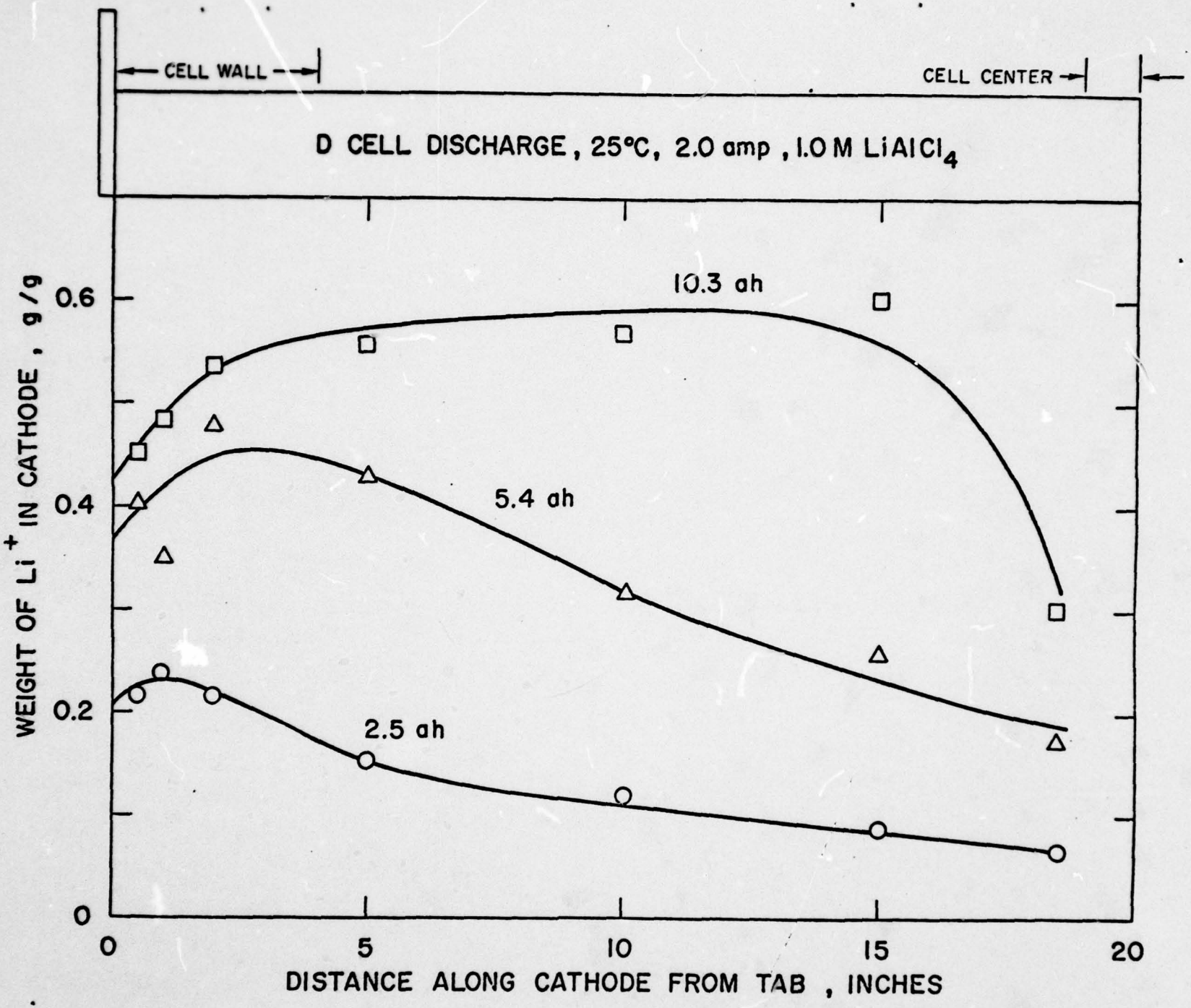

Fig. 5. Longitudinal reaction profiles of carbon cathode.

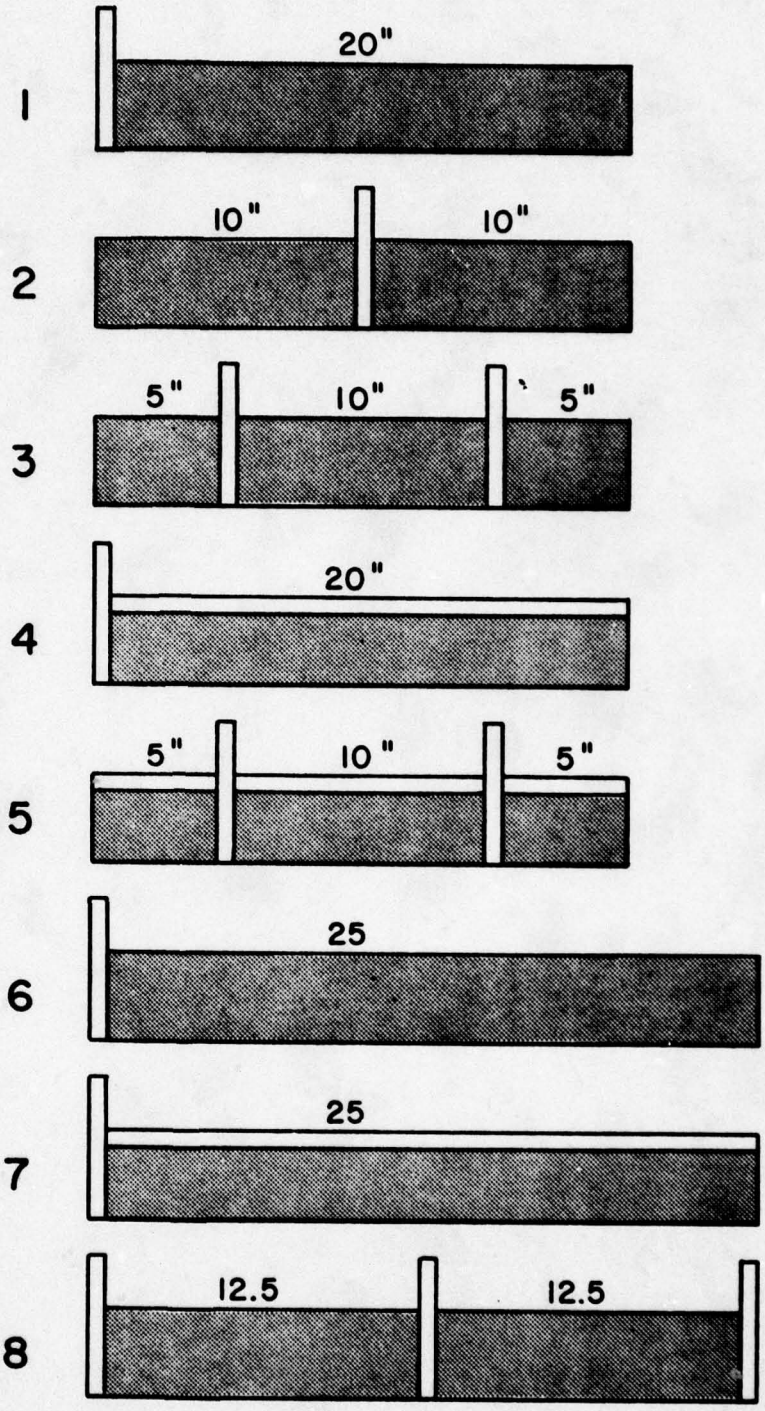

Fig. 6. Current collector designs of the carbon cathodes of spirally wound D cells.

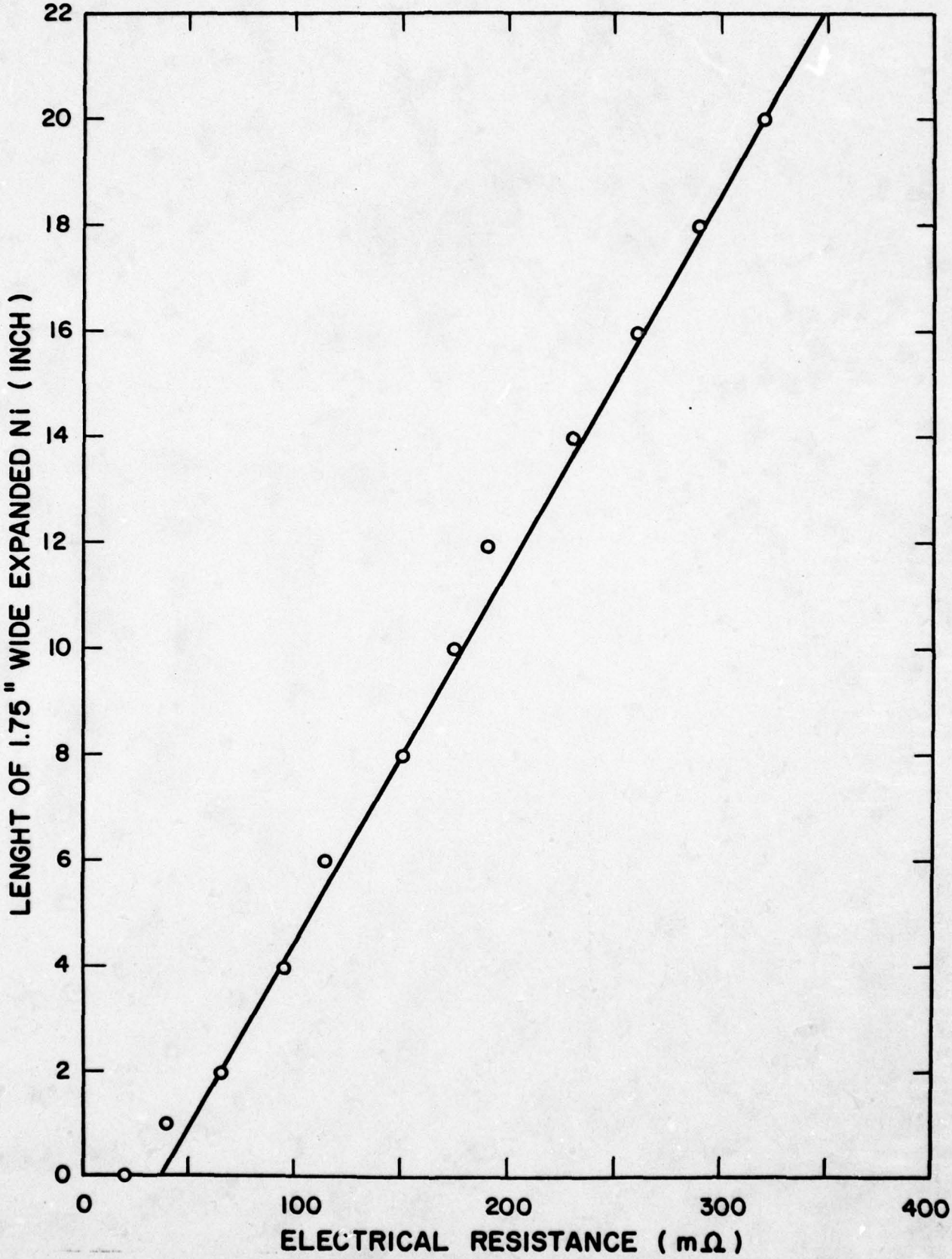

Fig. 7. Electrical resistance of expanded Ni cathode current collector.

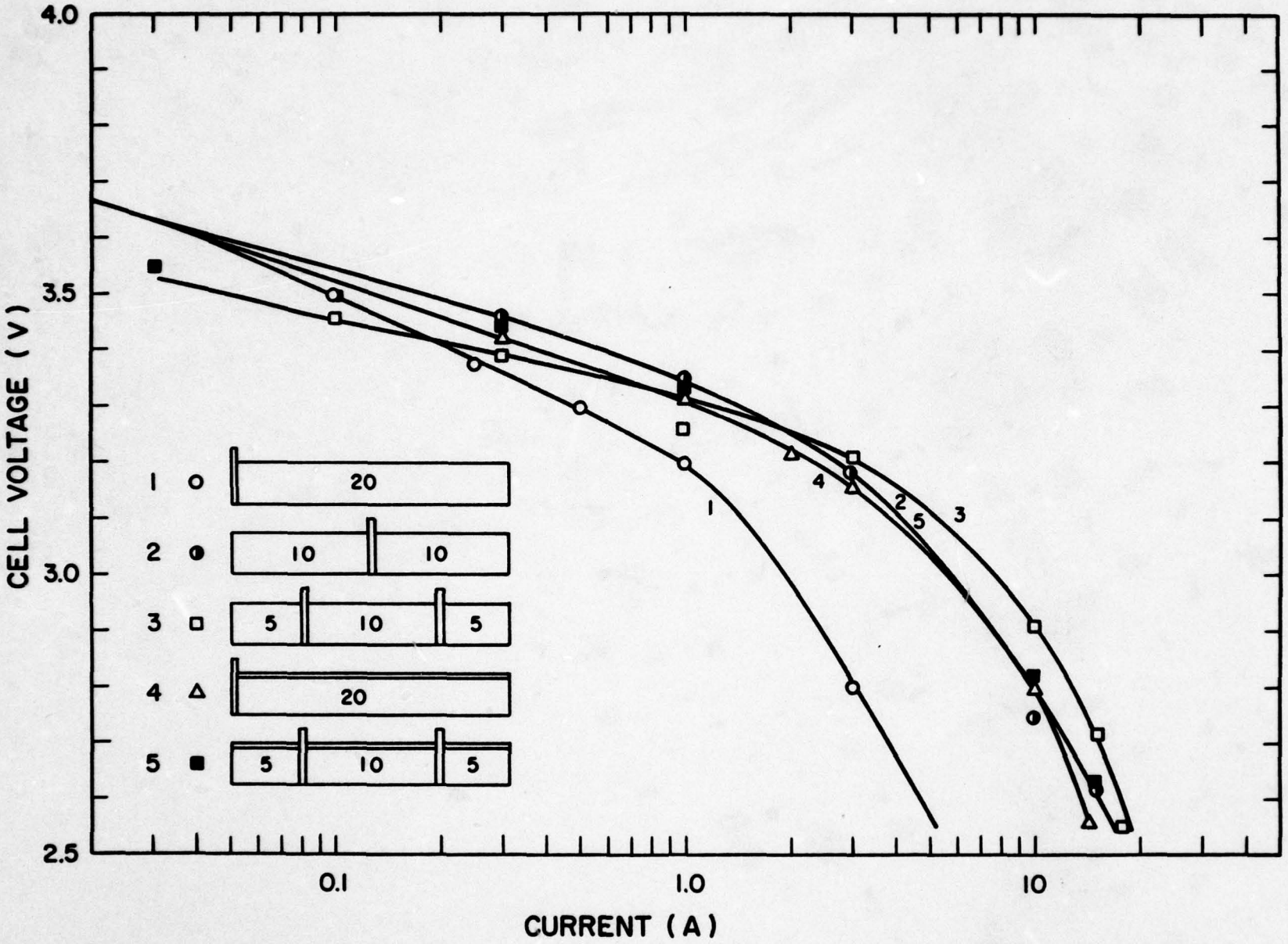

Fig. 8. Polarization characteristics of D cells with 20 inch cathodes of various current collector designs.

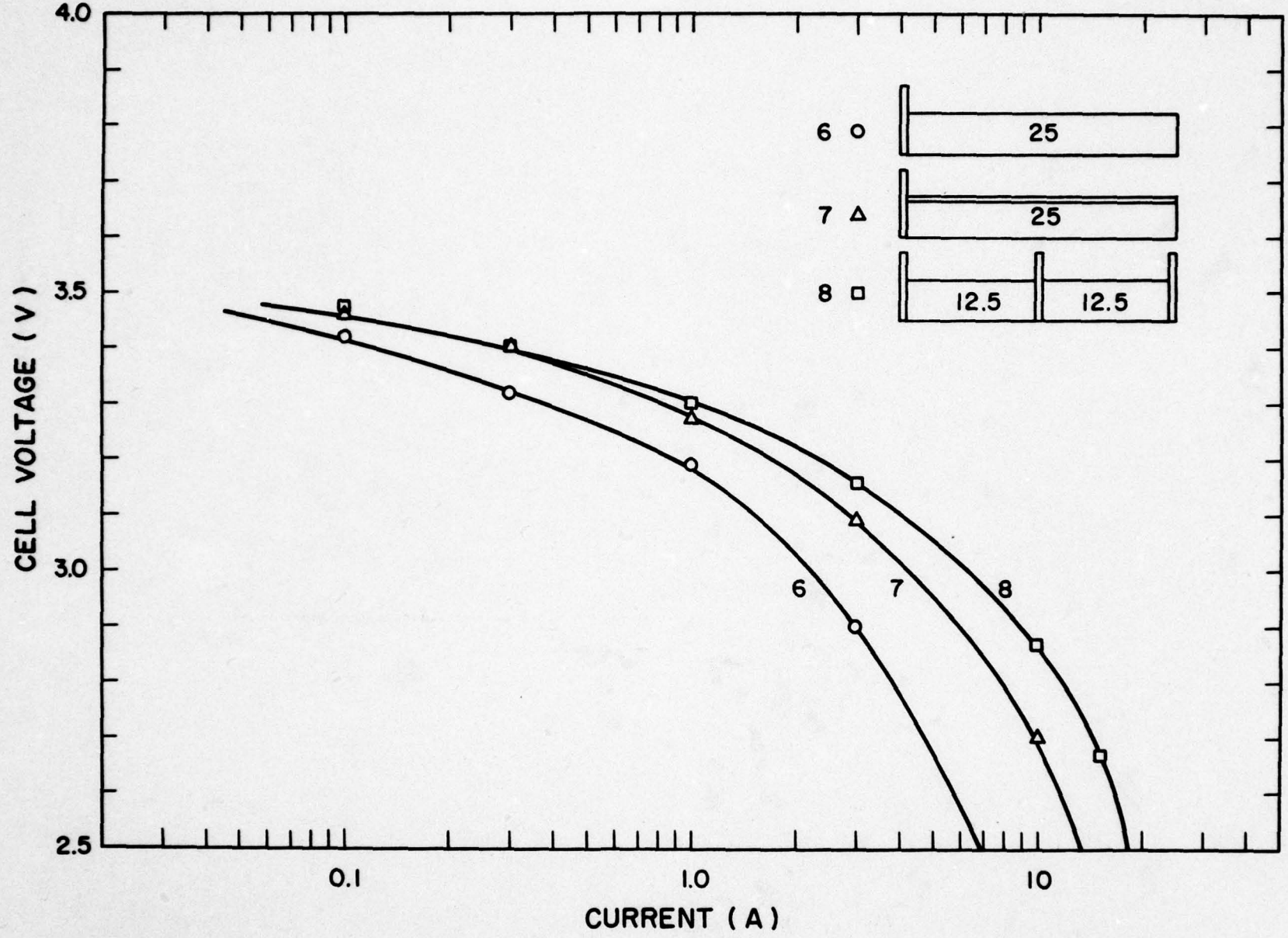

Fig. 9. Polarization characteristics of D cells with 25 inch long cathodes of various current collector design.

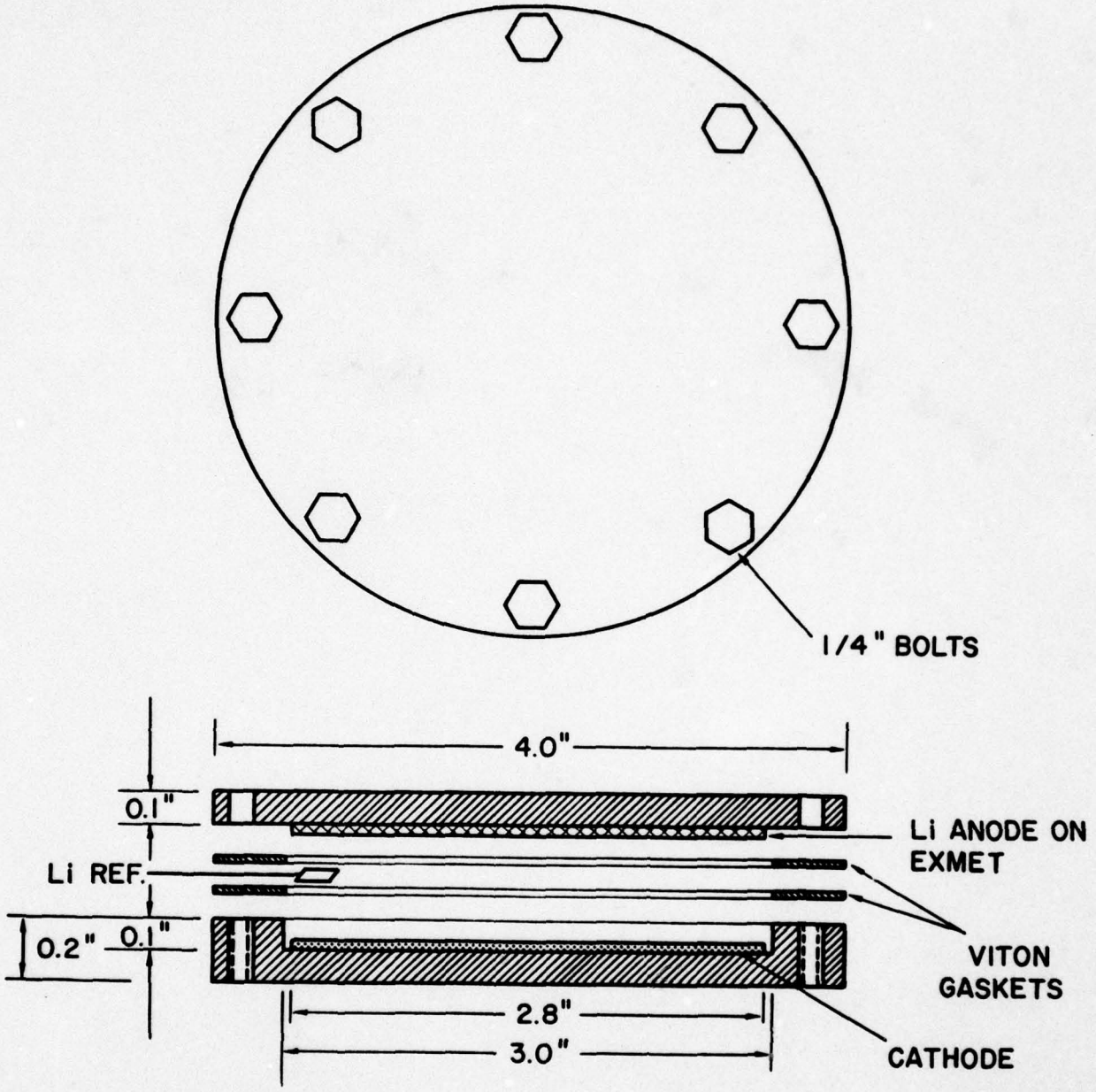

Fig. 10. Schematic view of the experimental demountable flat cylindrical cell.

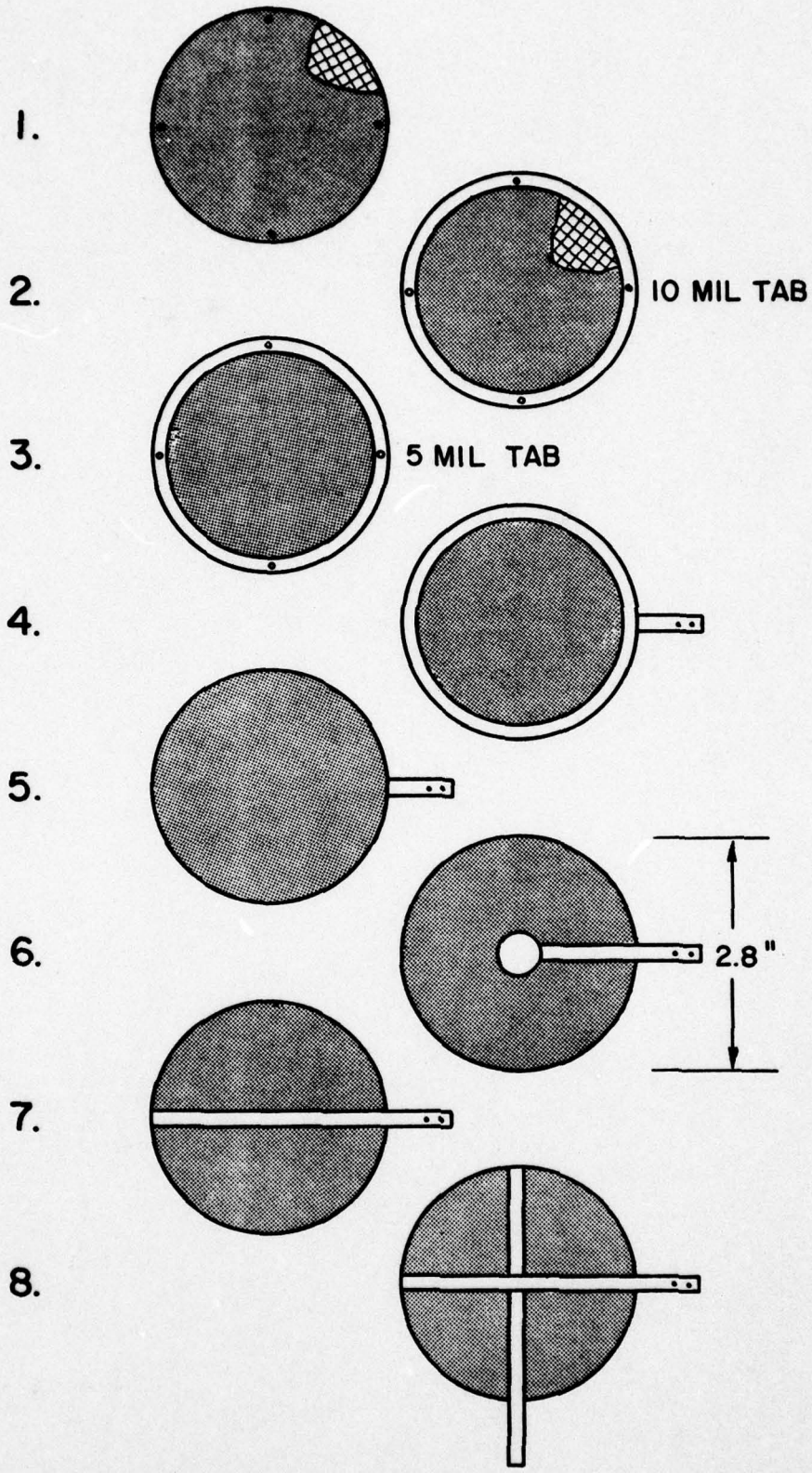

Fig. 11. Current collector designs for the 2.8 inch diameter disc cathodes.

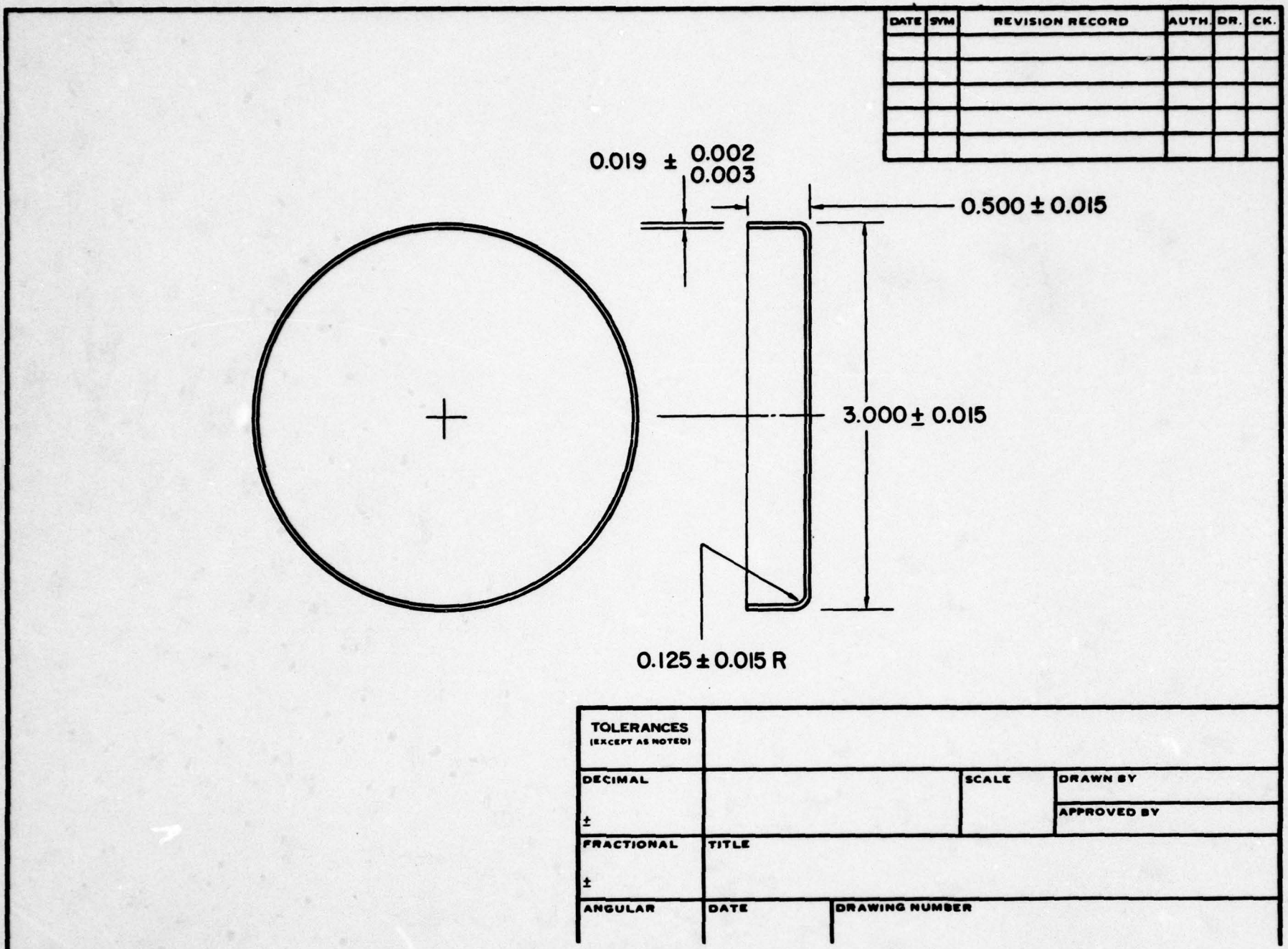

Fig. 12. Flat cylindrical cell container.

DATE	SYM	REVISION RECORD	AUTH.	DR.	CK.

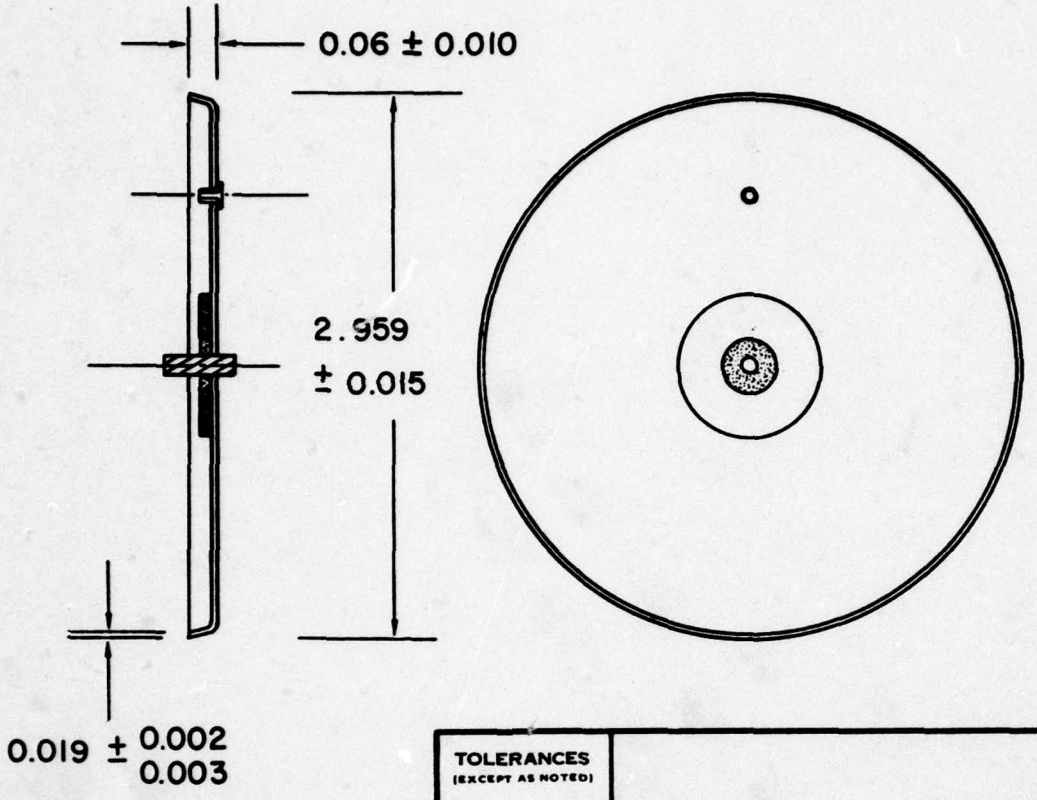

TOLERANCES (EXCEPT AS NOTED)			
DECIMAL ±		SCALE	DRAWN BY APPROVED BY
FRACTIONAL ±	TITLE		
ANGULAR	DATE	DRAWING NUMBER	

Fig. 13. Flat cylindrical cell top with G/M seal and the electrolyte fill port.

DATE	SYM	REVISION RECORD	AUTH.	DR.	CK.

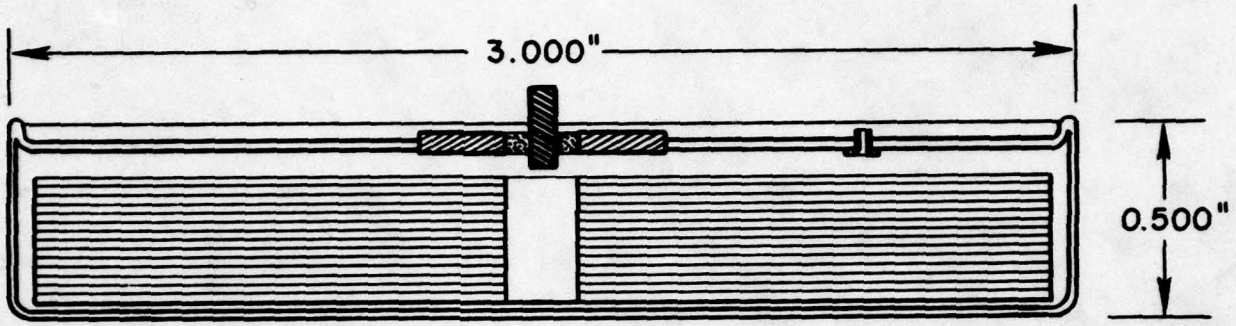

TOLERANCES (EXCEPT AS NOTED)			
DECIMAL ±		SCALE	DRAWN BY
			APPROVED BY
FRACTIONAL ±	TITLE		
ANGULAR	DATE	DRAWING NUMBER	

Fig. 14. Cross-Sectional view of the hermetic flat cylindrical cell.

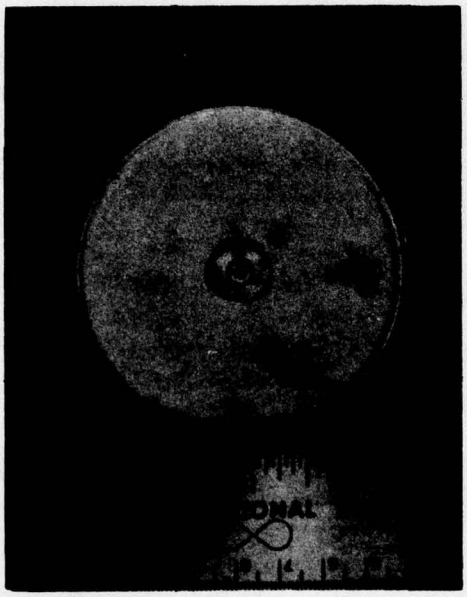

Fig. 15. Photograph of a hermetic flat cylindrical cell.

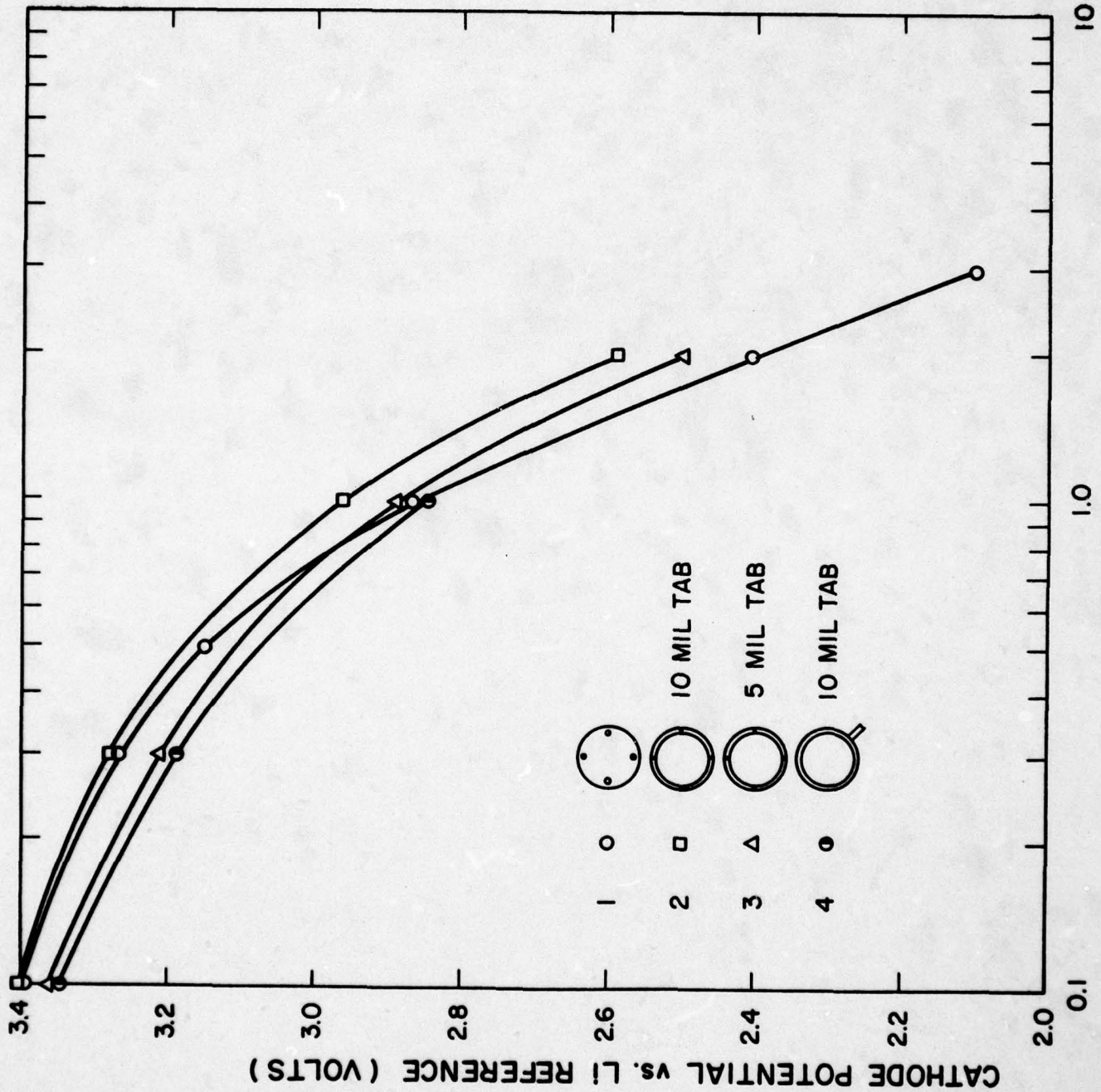

Fig. 16. Polarization characteristics of disc shaped cathodes with various current collector designs.

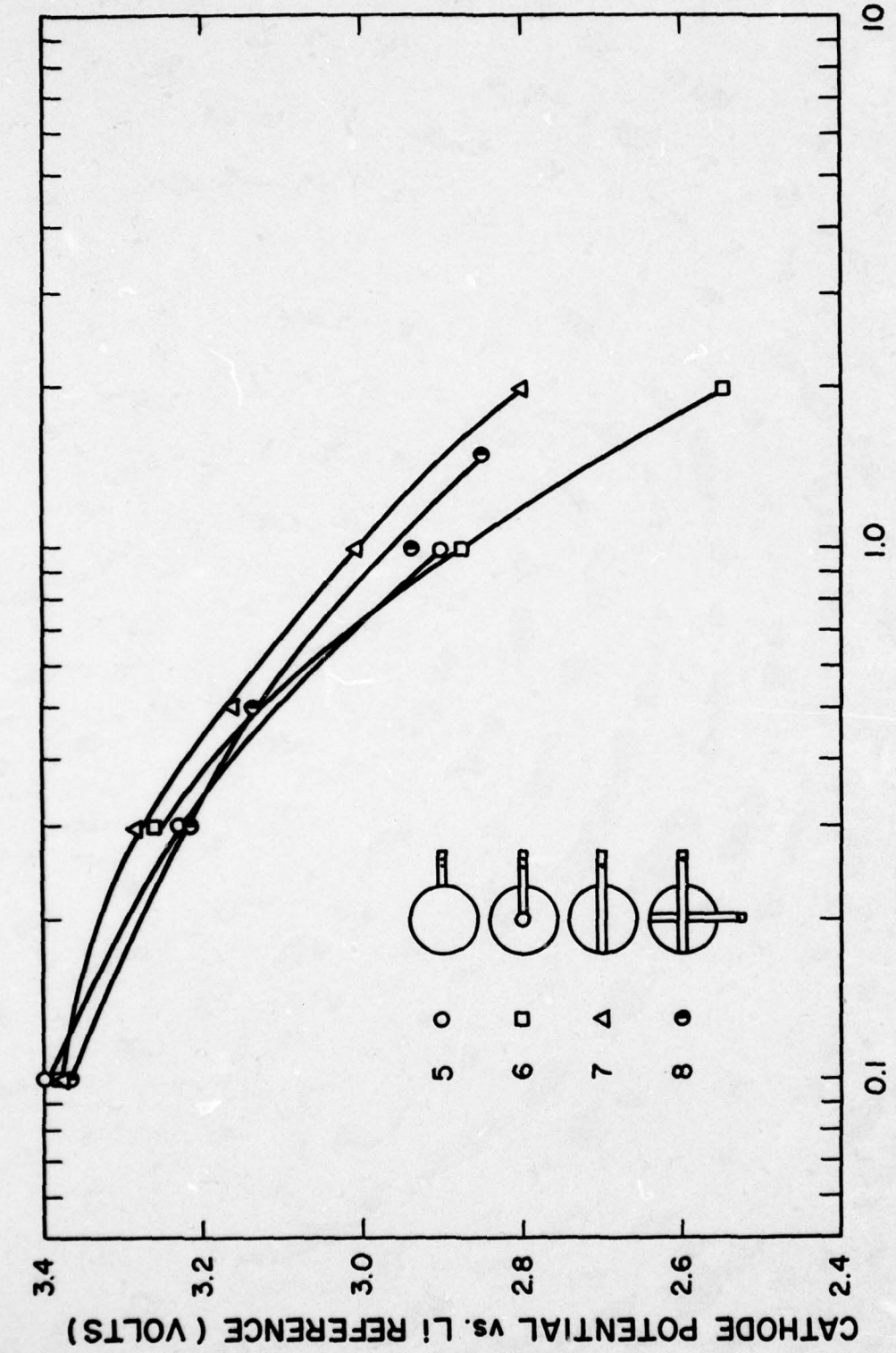

Fig. 17. Polarization characteristics of disc shaped cathodes with various current collector designs.

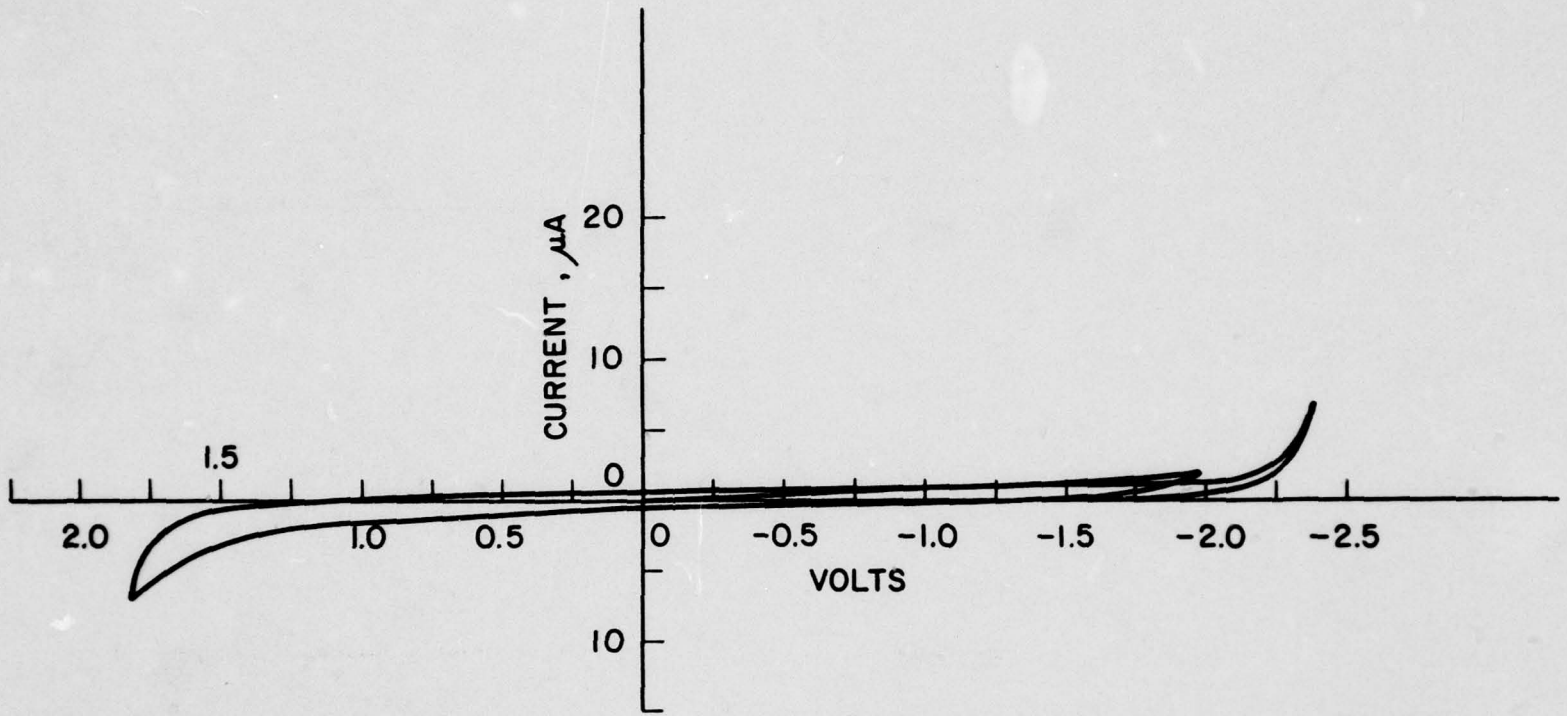

Fig. 18. Cyclic voltammograms of tetrabutyl ammonium hexafluorophosphate solution in acetonitrile on Pt electrode, background, scan rate 200 mv/sec.

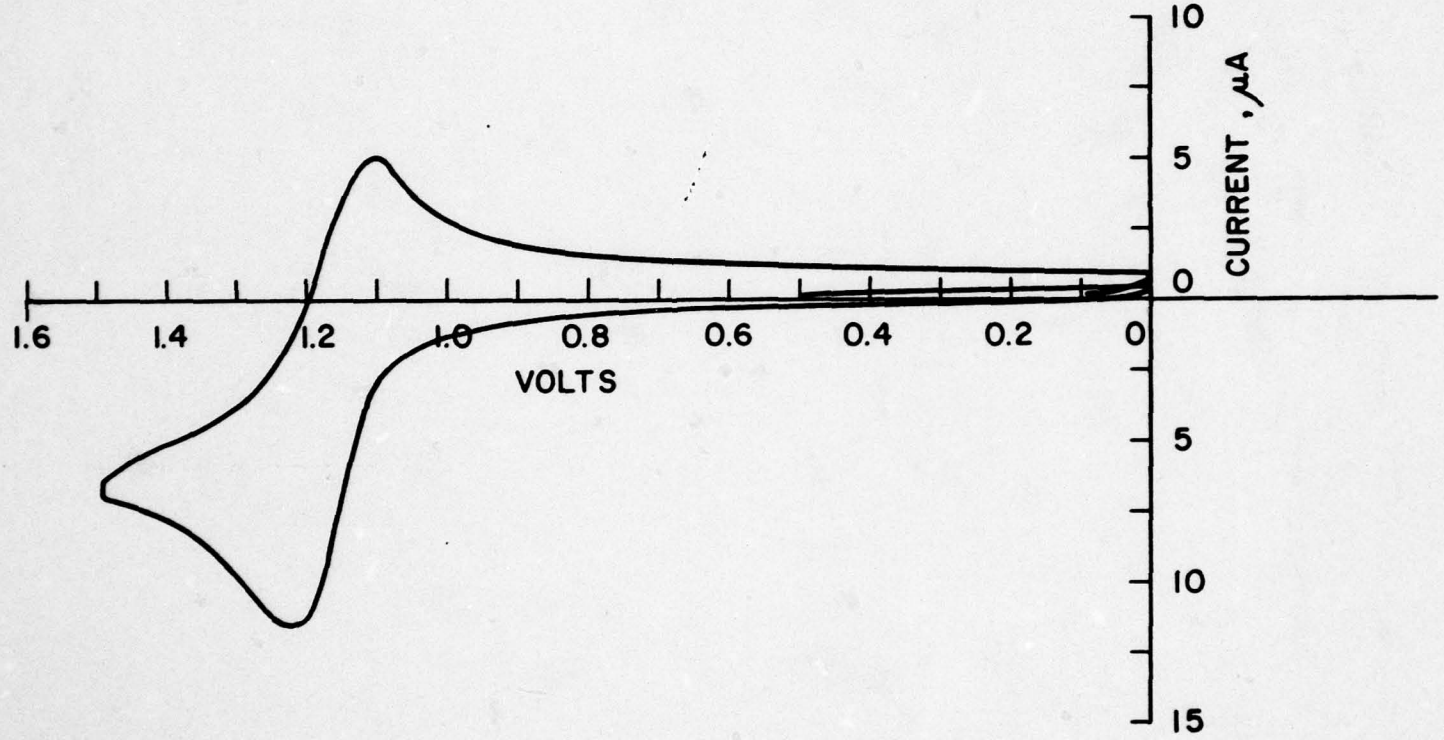

Fig. 19. Cyclic voltammogram of tetramethyl ammonium chloride in acetonitrile/tetrabutyl ammonium hexafluorophosphate, scan rate 200 mv/sec.

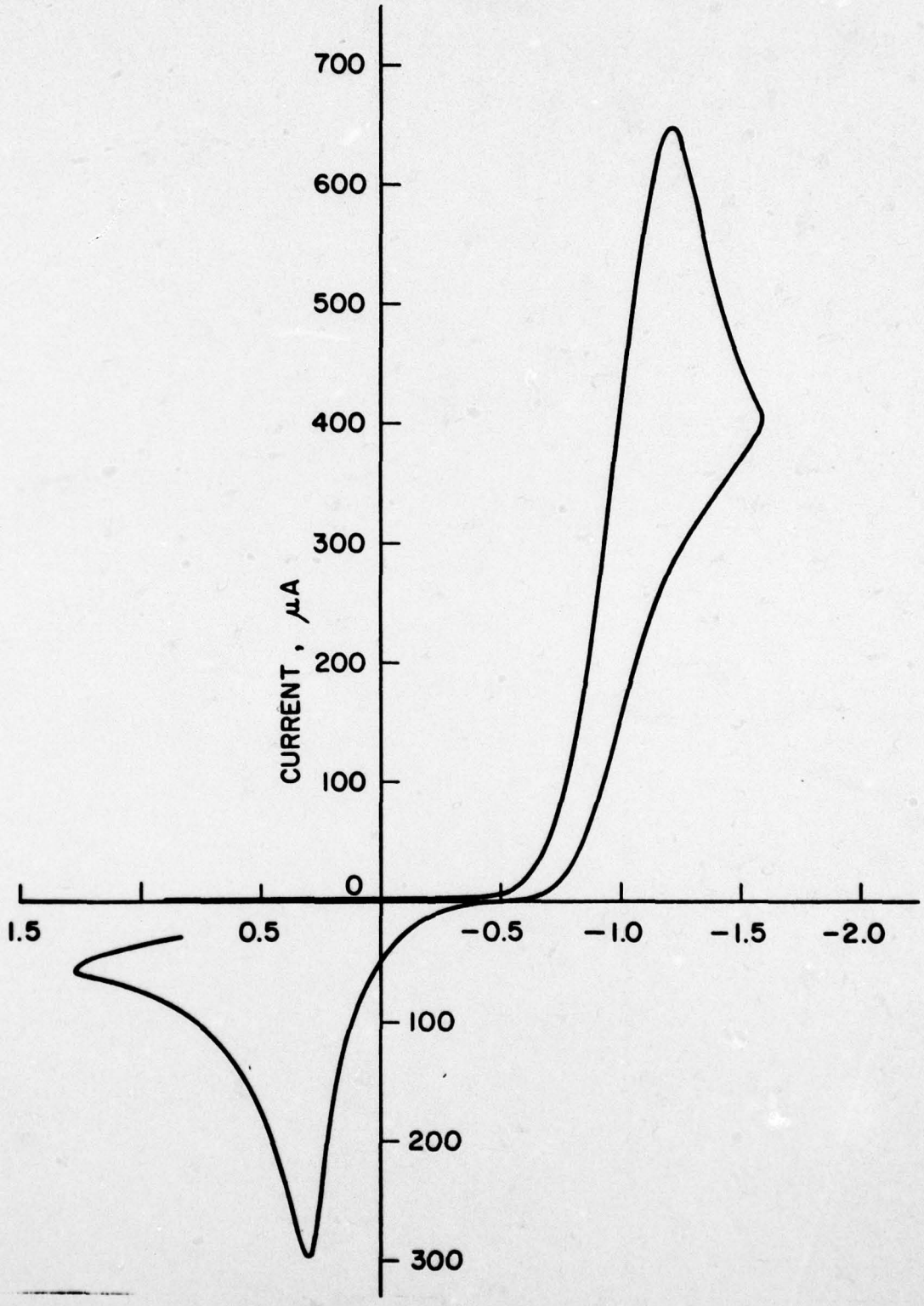

Fig. 20. Cyclic voltammogram of SO_2 in acetonitrile/tetrabutyl ammonium hexafluorophosphate, scan rate 1v/sec.

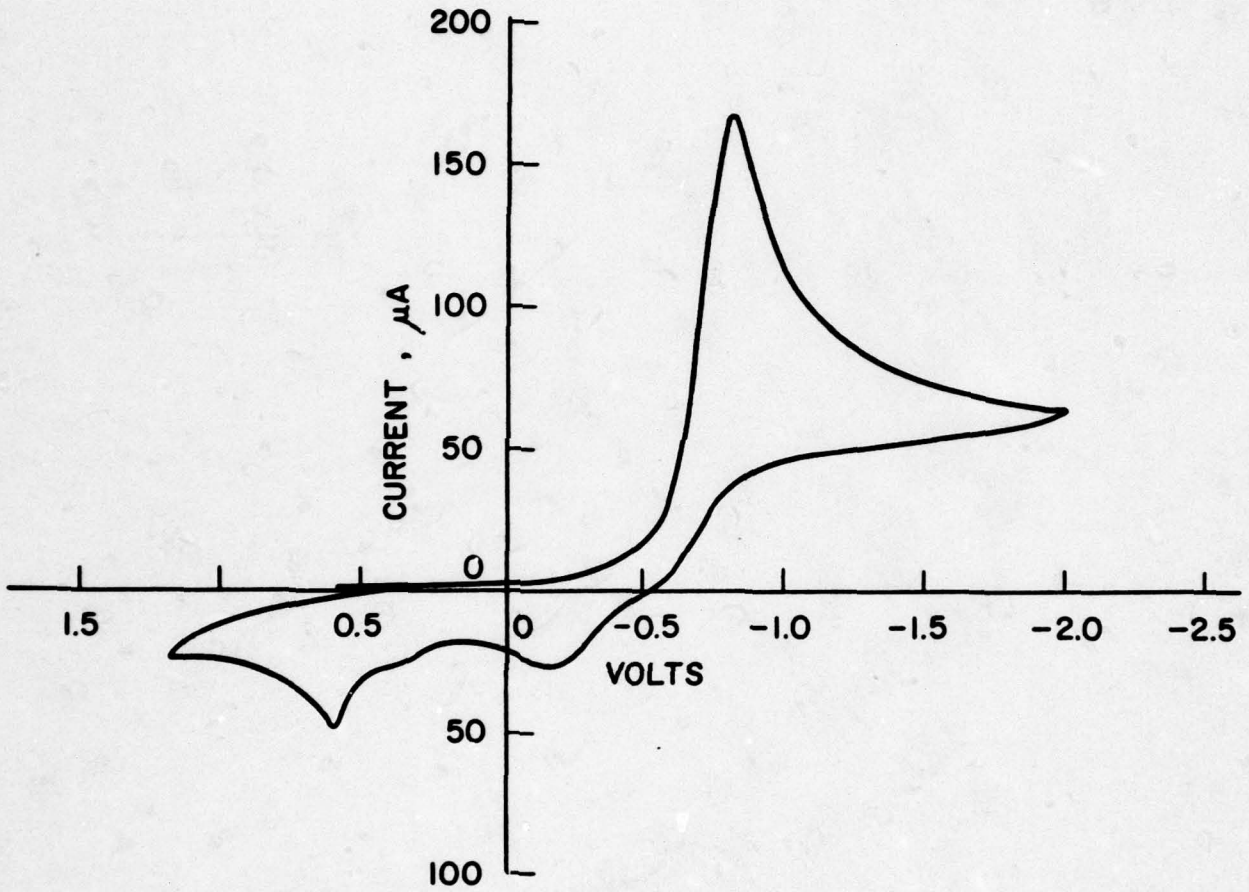

Fig. 21. Cyclic voltammogram of SO_2 in dimethyl formamide (DMF)/tetrabutyl ammonium hexafluorophosphate; scan rate 200 mv/sec.

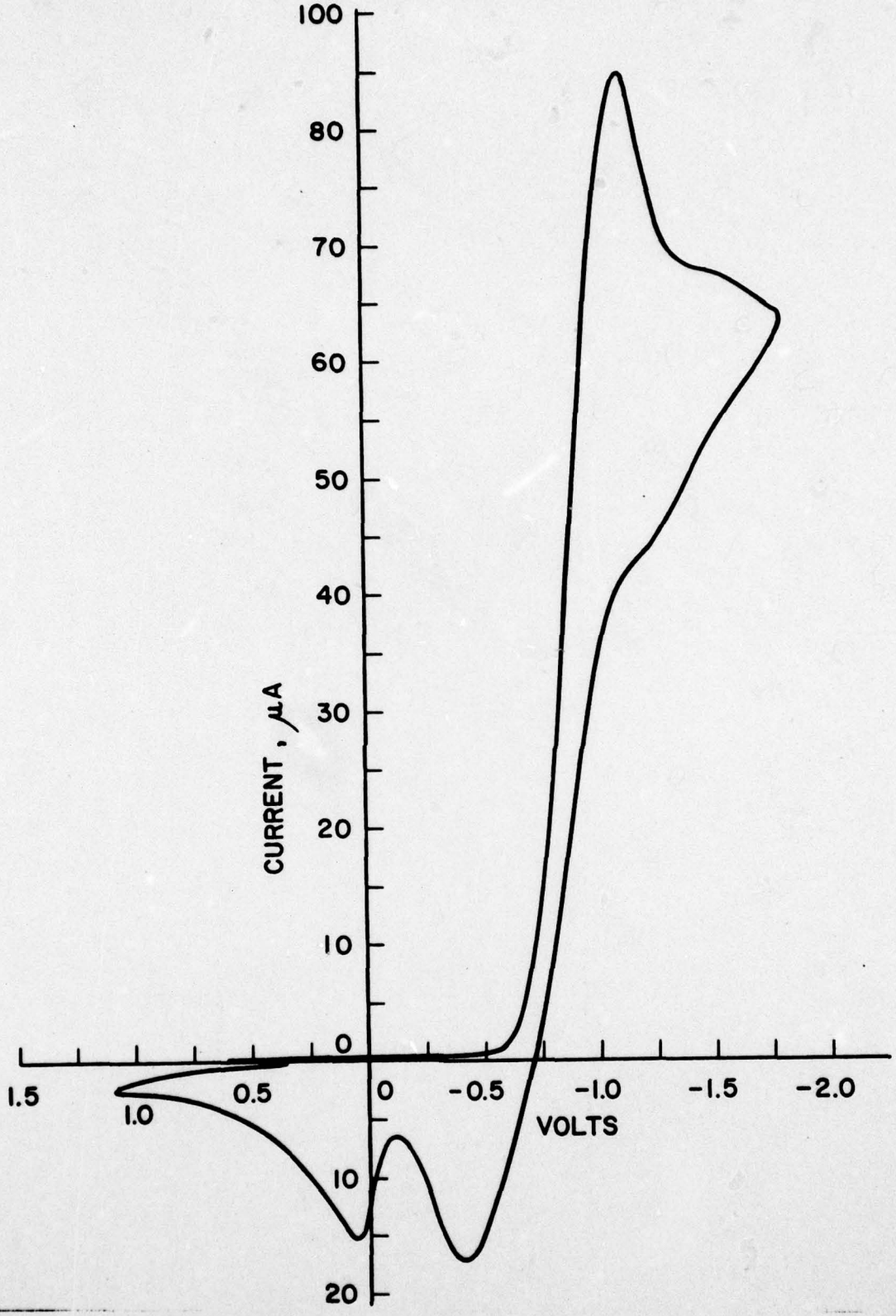

Fig. 22. Cyclic voltammogram of SO_2 in methylene chloride/ tetrabutyl ammonium hexafluorophosphate ($TBAPF_6$), scan rate 100 mv/sec.

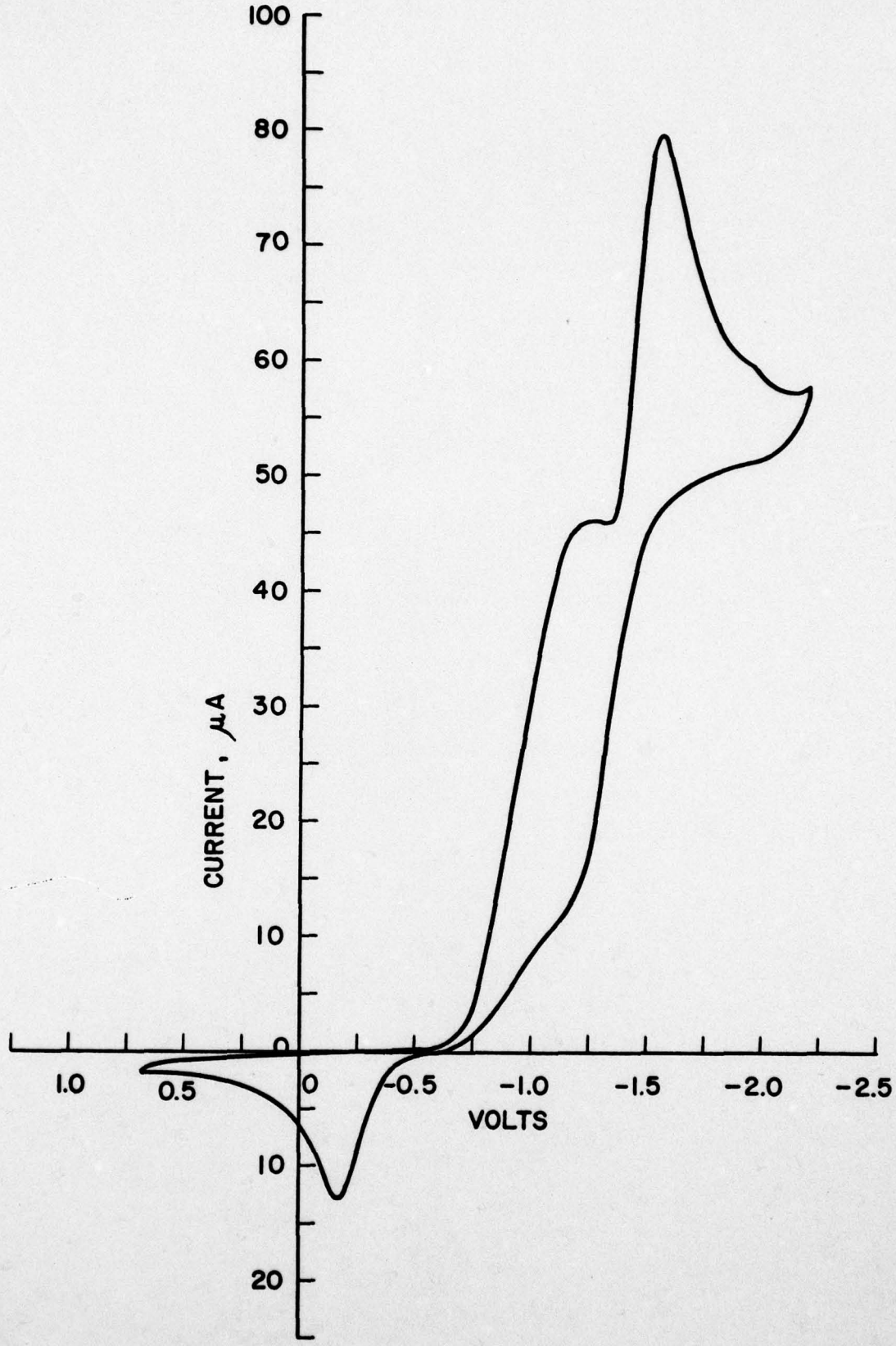

Fig. 23. Cyclic voltammogram of S in methylene chloride/ $TBAPF_6$, scan rate 200 mv/sec.

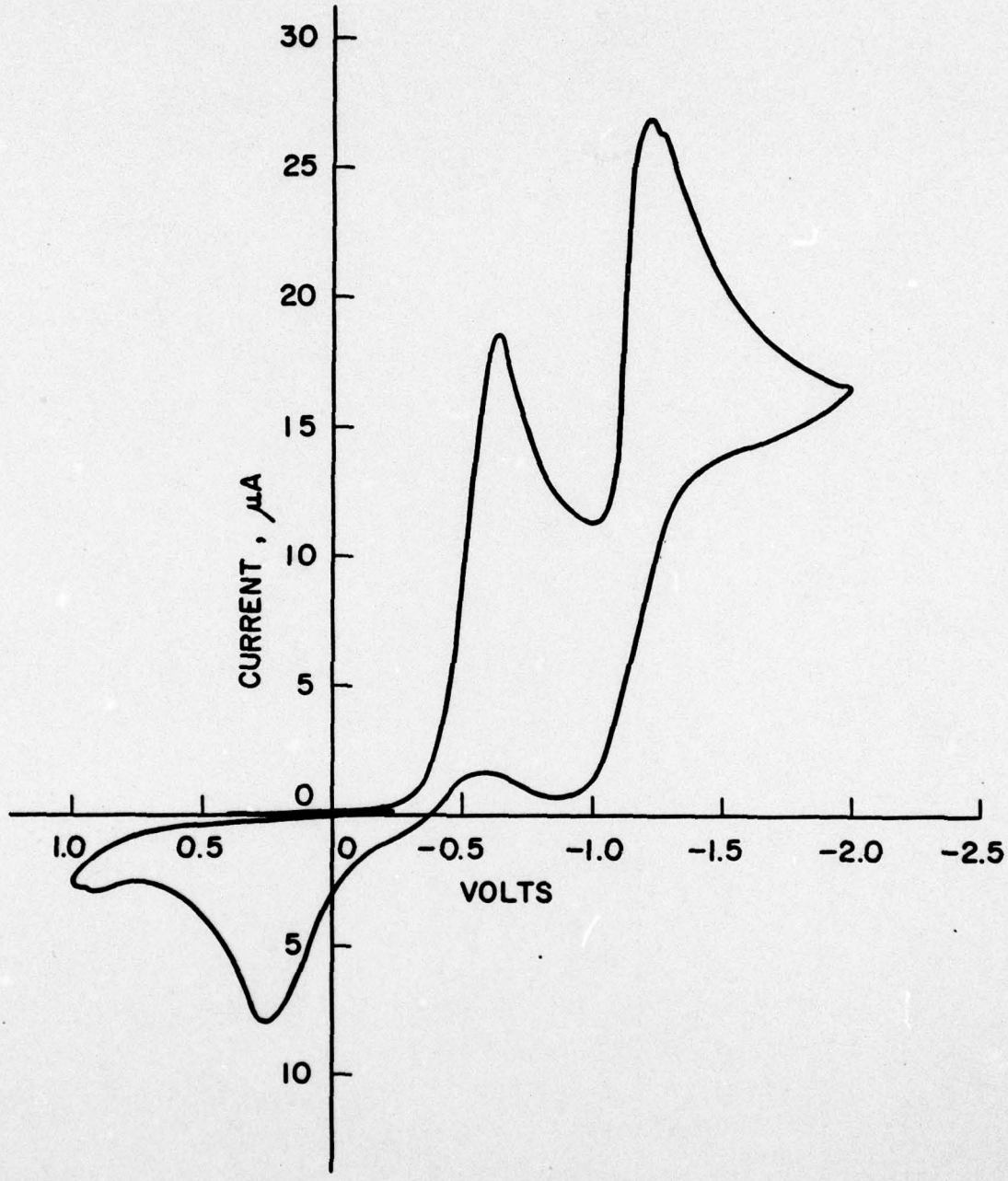

Fig. 24. Cyclic voltammogram of S in DMF/$TBAPF_6$, scan rate 500 mv/sec.

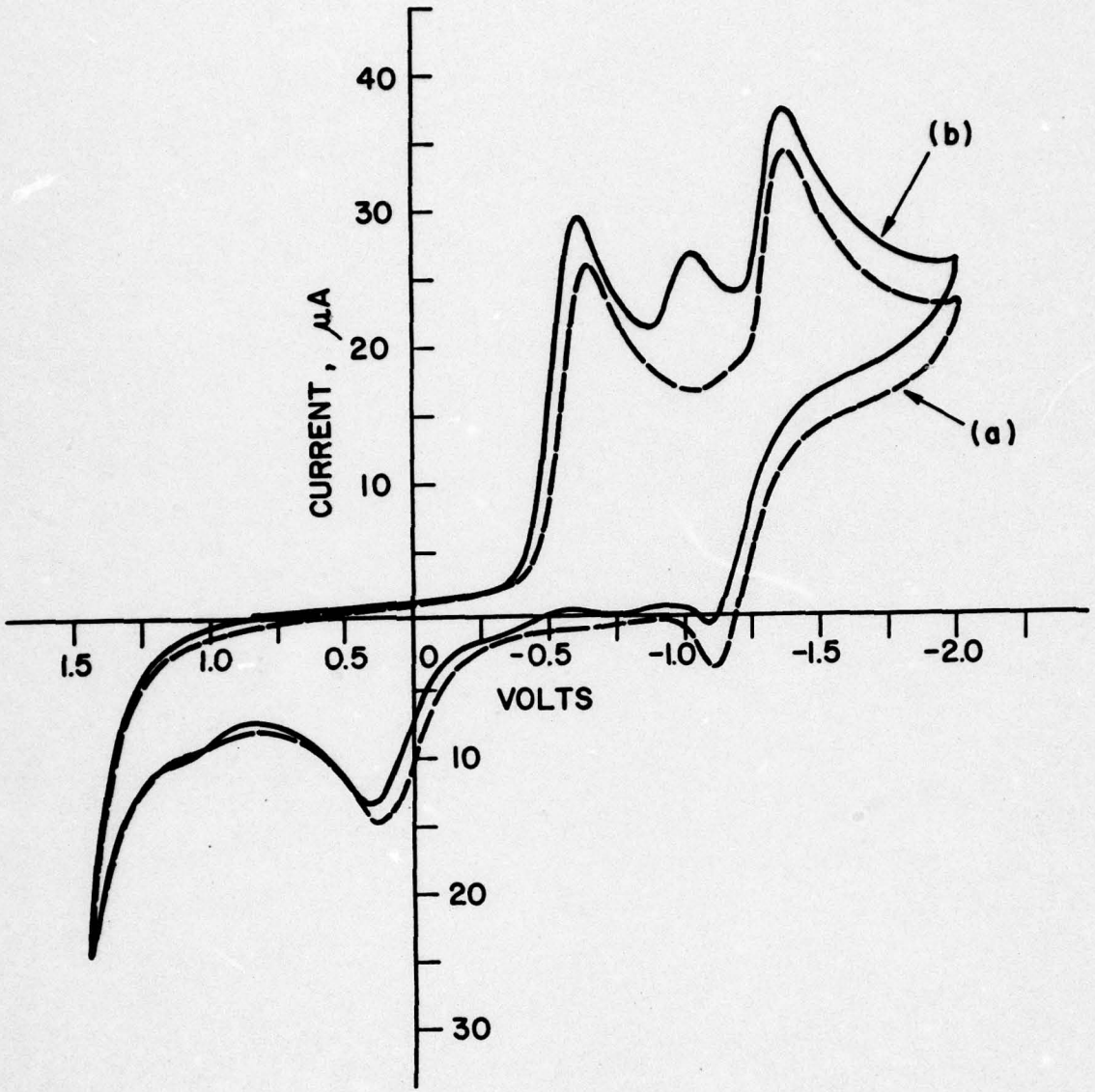

Fig. 25. Cyclic voltammograms of (a) S + trace SO_2 in DMF/$TBAPF_6$, (b) S + more SO_2 in DMF/$TBAPF_6$, scan rate 200 mv/sec.

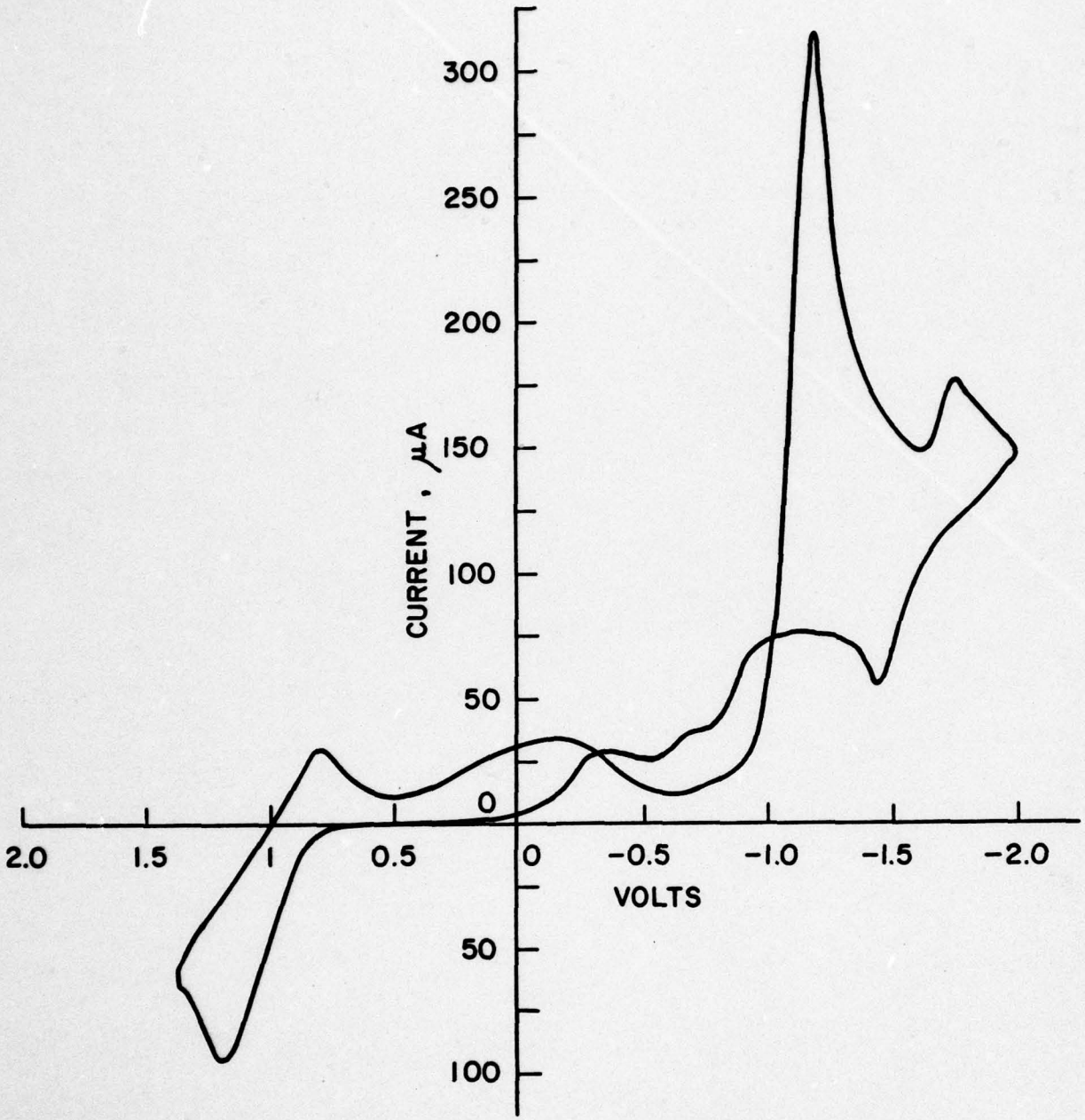

Fig. 26. Cyclic voltammogram of S_2Cl_2 in acetonitrile/$TBAPF_6$, scan rate 500 mv/sec.

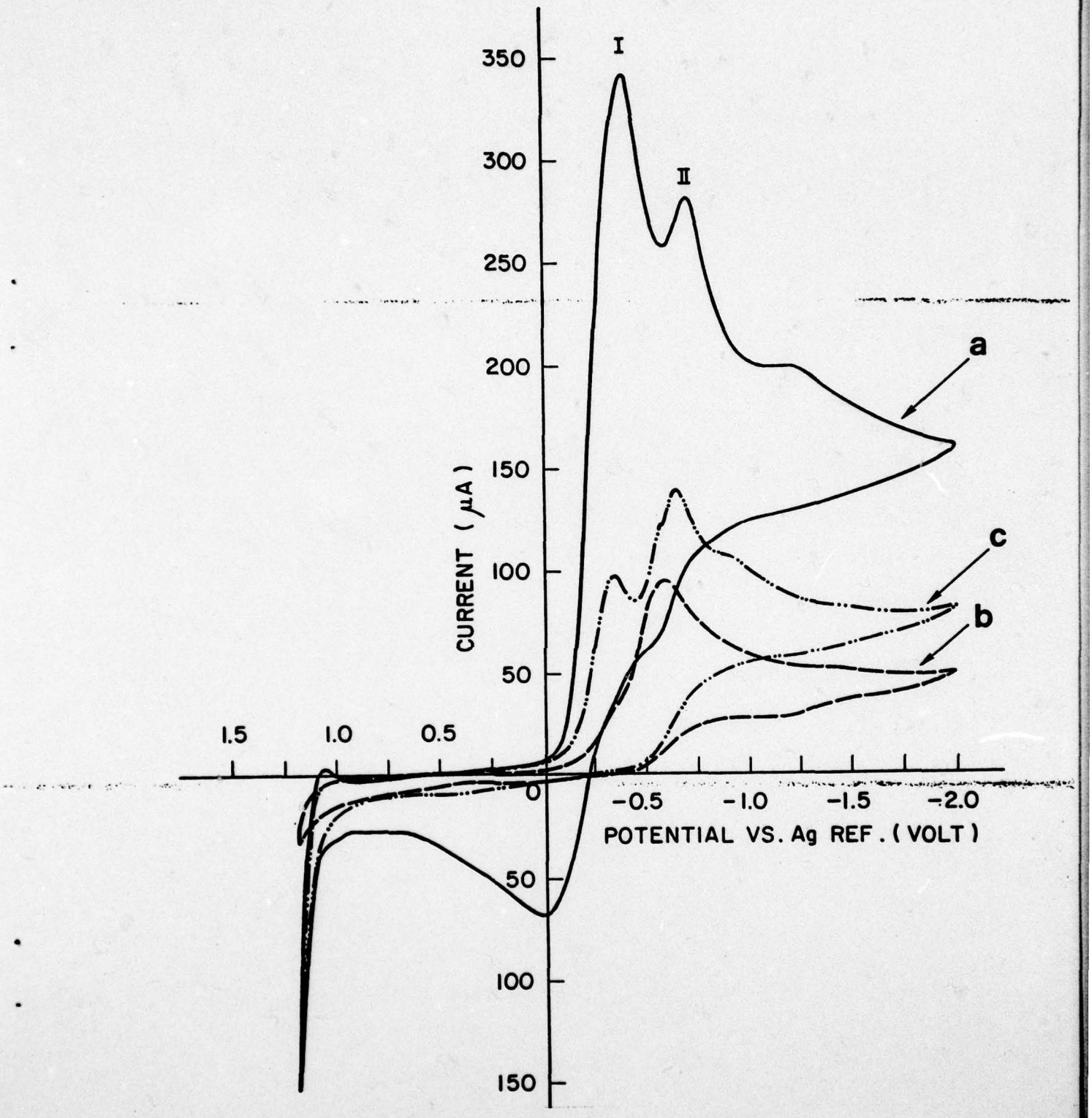

Fig. 27. Cyclic voltammograms of $SOCl_2$ in DMF/$TBAPF_6$ (a) before the electrolysis, (b) immediately after the exhaustive electrolysis at -0.25V vs Ag wire reference, (c) after warming the electrolyzed solution; scan rate 200 mv/sec.

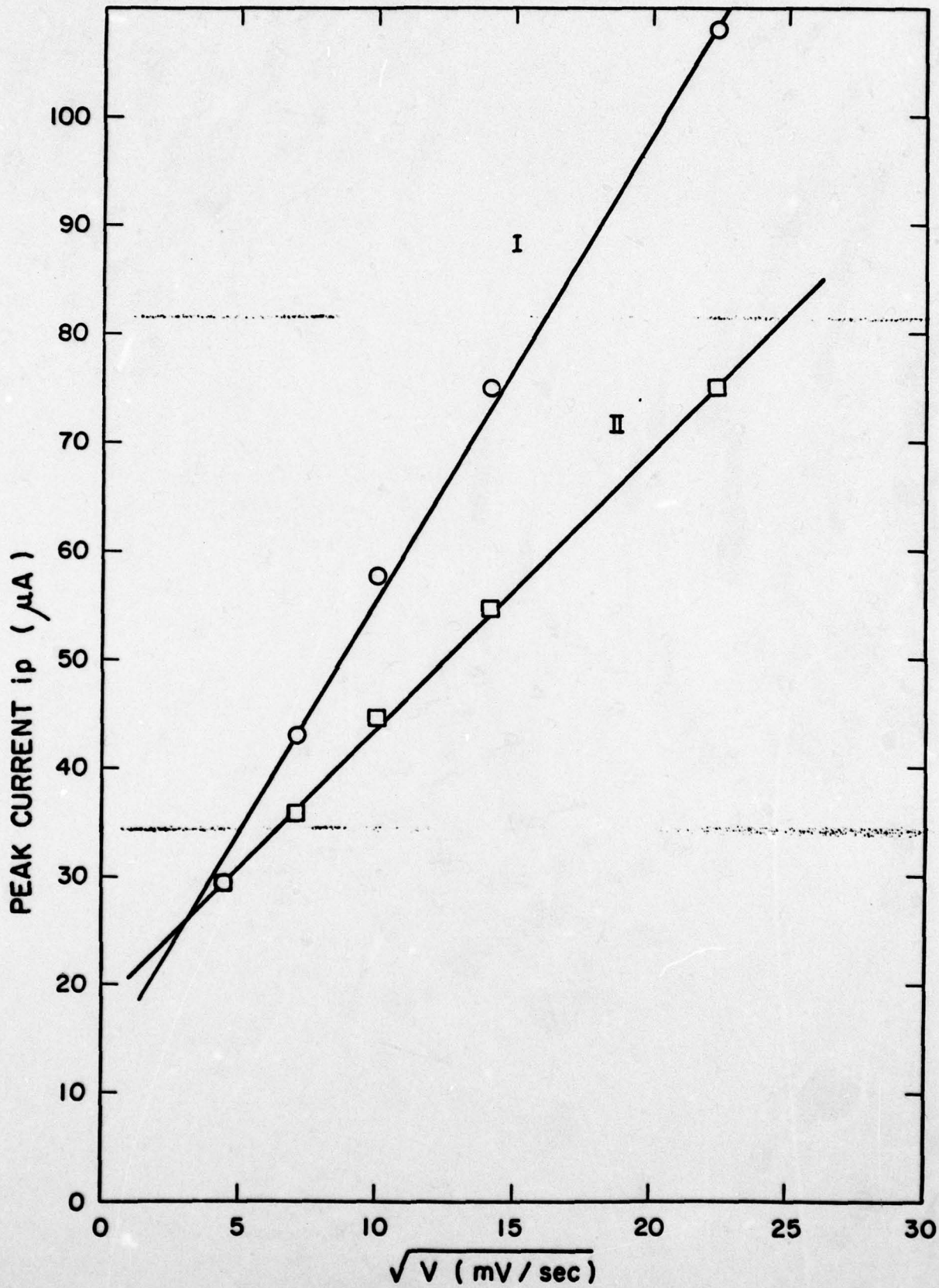

Fig. 28. Plot of the peak currents versus the square root of the scan rate (V) of the two reduction waves of $SOCl_2$ in DMF/$TBAPF_6$.

DISTRIBUTION LIST

Defense Documentation Center (12)
ATTN: DDC-TCA
Cameron Station (Bldg 5)
Alexandria, VA 22314

Commander (1)
Naval Ocean Systems Center
ATTN: Library
San Diego, CA 92152

CDR, Naval Surface Weapons Center (1)
White Oak Laboratory
ATTN: Library CODE WX-21
Silver Spring, MD 20910

Commandant, Marine Corps (2)
HQ US Marine Corps
ATTN: Code LMC
Washington, DC 20380

Rome Air Development Center (1)
ATTN: Documents Library (TILD)
Griffiss AFB, NY 13441

Air Force Geophysics Lab/SULL (1)
ATTN: S-29
Hanscom AFB, MA 01731

HQDA (DAMA-ARZ-D/DR. F.D. Verderame) (1)
Washington, DC 20310

CDR, Harry Diamond Laboratories (1)
ATTN: Library
2800 Powder Mill Road
Adelphi, MD 20783

Director (1)
US Army Material Systems Analysis ACTV.
ATTN: DRXSY-MP
Aberdeen Proving Ground, MD 21005

CDR, US Army Research Office (1)
ATTN: DRXRO-IP
P. O. Box 12211
Research Triangle Park, NC 27709

CDR, US Army Signals Warfare Lab (1)
ATTN: DELSW-OS
Vint Hill Farms Station
Warrenton, VA 22186

Commander (1)
US Army Mobility Eqp Res & Dev CMD
ATTN: DRDME-R
Fort Belvoir, VA 22060

Commander
US Army Electronics R&D Command
Fort Monmouth, NJ 07703

DELET-P	(1)
DELET-DD	(1)
DELET-DT	(2)
DELSD-L (TECH LIB)	(1)
DELSD-L-S (STINFO)	(2)
DELET-PR	(8)

Commander
US Army Communications R&D Command
Fort Monmouth, NJ 07703

USMC-LNO (1)

NASA Scientific & Tech Info Facility (1)
Baltimore/Washington Intl Airport
PO Box 8757, MD 21240

SUPPLEMENT TO DISTRIBUTION LIST

13 January 1978

Other Recipients

Mr. Donald Mortel (1)
AF Aero Propulsion Lab
ATTN: AFAPL-POE-1
Wright-Patterson AFB,
Ohio 45433

Mr. Richard E. Oderwald (1)
Department of the Navy
Hqs., US Marine Corps
Code LMC 4
Washington, DC 20380

Commander (1)
Harry Diamond Laboratories
ATTN: DELHD-RDD
(Mr. A. Benderly)
2800 Powder Mill Road
Adelphi, MD 20783

Distribution List Continued

Transportation Systems Center (1)
Kendall Square
Cambridge, MA 02142
ATTN: Dr. Norman Rosenberg

GTE Laboratories, Inc. (1)
40 Sylvan Road
Waltham, MA 02154

Foote Mineral Company (1)
Route 100
Exton, PA 19341
ATTN: Dr. H. Grady

Honeywell, Inc. (1)
104 Rock Road
Horsham, PA 19044
ATTN: C. Richard Walk

Sanders Associates, Inc. (1)
Sonobuoy Division
95 Canal Street
Nashua, N.H. 03060
ATTN: Mr. David Dwyer

Eagle-Picher Industries, Inc. (1)
Electronics Division
ATTN: Mr. Robert L. Higgins
P. O. Box 47
Joplin, Missouri 64801

Yardney Electric Company (1)
82 Mechanic Street
Pawcatuck, CT 02891
ATTN: Mr. William E. Ryder

Exxon Research & Engineering Co. (1)
Corporate Research Laboratory
Linden, N.J. 07036
ATTN: Dr. R. Hamlen

Argonne National Laboratories (1)
9700 South Cass
Argonne, IL 60439
ATTN: Dr. E. C. Gay

GTE Sylvania, Inc. (1)
77 A Street
Needham Heights, MA 02194
ATTN: Mr. Richard Pabst

General Motors Corp. (1)
Research Laboratories
General Motors Technical Center
12 Mile and Mound Roads
Warren, MI 48090
ATTN: Dr. J. L. Hartman

Union Carbide Corporation (1)
Parma Research Center
P. O. Box 6116
Cleveland, OH 44101

P. R. Mallory & Co. Inc. (1)
South Broadway
Tarrytown, N.Y. 10591
ATTN: J. Dalfonso

North American Rockwell Corp. (1)
Atomics International Division
Box 309
Canoga Park, CA 91304
ATTN: Dr. L. Heredy

General Electric Rsearch & (1)
Development Center
P. O. Box 8
Schenectady, N.Y. 12301
ATTN: Dr. Stefan Mitoff

University of California (1)
Department of Science & Research
Santa Barbara, CA 93100
ATTN: Dr. J. Kennedy

The Electric Storage Battery Co. (1)
Carl F. Norburg Research Center
19 W. College Avenue
Yardley, PA 19067
ATTN: Dr. A. Salkind

Gulton Industries, Inc. (1)
Metuchen, N.J. 08840
ATTN: Mr. S. Charlip

Electrochimica (1)
2485 Charleston Road
Mountain View, CA 94040
ATTN: Dr. Eisenberg

Distribution List Continued

Dr. Hugh Barger (1)
P. O. Box 2232
Davidson, NC 28036

Energy Storage & Donversion Dept. (1)
TRW Systems
One Space Park
Redondo Beach, CA 90278
ATTN: Dr. H. P. Silverman

Sanders Associates, Inc. (1)
24 Simon Street
Mail Stop NSI-2208
Nashua, NH 03060
ATTN: J. Marshall

Power Conversion, Inc. (1)
70 MacQuesten Pkwy
Mount Vernon, NY 10550
ATTN: Stuart Chodosh

Dr. D. Pouli (1)
Portfolio Manager
Hooker Chemicals & Plastics Corp.
M.P.O. Box 8
Niagara Falls, NY 14302

Dr. Leonard Nanis (1)
G207
S.R.I. Menlo Park, CA 94025

Dr. J. J. Auborn, RM 1A-317 (1)
Bell Laboratories
600 Mountain Avenue
Murray Hill, N.J. 07974

Stonehart Associates, Inc. (1)
34 Five Fields Road
Madison, CT 06443
ATTN: Mr. Thomas Reddy

Frank Murphy/SB331 (1)
Naval Underwater Systems Center
Newport Laboratory
Newport, RI 02840

NASA Lewis Research Center (1)
Mail Stop 6-1
21000 Brookpark Road
Cleveland, OH 44135
ATTN: Dr. Stuart Fordyce

Mr. Joe McCartney (1)
Naval Undersea Center
Code 608
San Diego, CA 92132

EIC, Inc. (1)
ATTN: S. B. Brummer
Newton, MA 02158

Altus Corp. (1)
440 Page Mill Road
Palo Alto, CA 94360
ATTN: Douglas Glader

J. Bene (1)
MS 488
NASA Langley Research Center
Hampton, VA 23665

Mr. Eddie T. Seo (1)
Research and Development Div.
The Gates Rubber Co.
999 S. Broadway
Denver, CO 80217

Mr. Sidney Gross (1)
Mail Stop 8C-62
Boeing Aerospace Company
P. O. Box 3999
Seattle, WA 98124

Honeywell Technology Center (1)
ATTN: Dr. H. V. Venkatasetty
10701 Lyndale Avenue South
Bloomington, MN 55420